A Climatology of Southwest Indian Ocean Tropical Systems: their Number, Tracks, Impacts, Sizes, Empirical Maximum Potential Intensity and Intensity Changes

Marie-Dominique Leroux, Julien Meister, Dominique Mékies, Annie-Laure Dorla, Philippe Caroff

A Climatology of Southwest Indian Ocean Tropical Systems: Their Number, Tracks, Impacts, Sizes, Empirical Maximum Potential Intensity, and Intensity Changes

MARIE-DOMINIQUE LEROUX, JULIEN MEISTER, DOMINIQUE MEKIES, AND ANNIE-LAURE DORLA

Laboratoire de l'Atmosphère et des Cyclones (UMR 8105/CNRS, Université de La Réunion, Météo-France), Saint-Denis de La Réunion, France

PHILIPPE CAROFF

Regional Specialized Meteorological Centre La Réunion, Météo-France, Saint-Denis de La Réunion, France

(Manuscript received 8 April 2017, in final form 19 January 2018)

ABSTRACT

A 17-yr "climatology" of tropical-system activity, track, size, and 24-h intensity change in the southwest Indian Ocean (SWIO) is developed and analyzed in comparison with other intensively studied basins such as the North Atlantic Ocean. A first formulation of the empirical maximum potential intensity of SWIO tropical systems is also proposed, along with the climatology of sea surface temperatures from September to June. Systems with a 34-kt (1 kt = 0.514 m s^{-1}) wind radius that does not exceed 46 km are considered to be very small or midget systems, on the basis of the 5th percentile of storm size distribution. Using the 95th percentile of overwater intensity changes, rapid intensification (RI) is statistically defined by a minimum increase of 15.4 m s^{-1} day^{-1} in the maximum 10-min mean surface wind speed (VMAX). This value is similar to the 30-kt threshold commonly used in the North Atlantic basin for 1-min sustained wind speeds. Rapid decay (RD) can be statistically defined by a minimum weakening of 13.9 m s^{-1} day^{-1}, although the spread in the 5th percentile of intensity changes among the different intensity classes indicates that it is not as appropriate to use a unique RD threshold for all systems. It is shown that 43% of all tropical systems and all very intense tropical cyclones (VMAX $\geq$ 59.6 m s^{-1}) underwent RI at least once during their lifetimes. It is highlighted that systems have a greater propensity to intensify rapidly for an initial intensity between 65 and 75 kt. Statistics indicate that operational intensity forecast errors are significantly greater at short range for RI cases while track errors are reduced.

1. Introduction

The southwest Indian Ocean (SWIO) has been poorly studied so far despite having tropical-system activity that is comparable to that of the North Atlantic Ocean (NA) (WMO 2017). Under the responsibility of the Regional Specialized Meteorological Center (RSMC) of La Réunion for tropical-system warnings, this basin extends from the equator to 40°S and from the African coast (30°E) to 90°E. Tropical systems that form in this area can affect various Indian Ocean island nations and/or various countries along the eastern coast of Africa. Many systems strike vulnerable islands such as Madagascar (22 million inhabitants, with very fragile infrastructure and an agriculture-dominated economy) or the Mascarene Islands, which include La Réunion (870 000 inhabitants) and Mauritius (1.3 million inhabitants). Some countries are very poor and do not have adequate disaster-warning systems or risk-mitigation strategies. They can suffer from huge environmental, economic, and sanitary impacts. To support international efforts toward the improvement of tropical-system prediction, it is important to characterize the past and present tropical activity in the SWIO. Tropical activity may also evolve throughout the century in the context of a changing climate with increased greenhouse gas concentrations (Emanuel 2005; Elsner et al. 2008; Knutson et al. 2010, 2013). It will be our ultimate goal to address this latter issue in a future research project.

Observations are limited in the Indian Ocean, and organized field campaigns could provide insights and

Corresponding author: Marie-Dominique Leroux, marie-dominique.leroux@meteo.fr

DOI: 10.1175/JAMC-D-17-0094.1

refinements to the methods used in the SWIO. Best-track (BT) estimates of storm wind speed and position in the SWIO are likely not as robust as in other basins that benefit from aircraft reconnaissance (e.g., Velden et al. 2006). The tools and methods for estimating intensity estimates (in terms of 10-min average maximum wind speeds) have naturally evolved with time. Subjective Dvorak estimates (Dvorak 1984) were the primary source of BT intensity estimates in the SWIO beginning around 1981–82. Since the 2000s, information from satellite scatterometers and passive microwave imagery has provided additional, valuable track and intensity information. Nowadays, an increasing number of BT intensities are based on blended data that include subjective Dvorak estimates, objective guidance [e.g., the advanced Dvorak technique (Olander and Velden 2007), the Advanced Microwave Sounding Unit (e.g., Brueske and Velden 2003), and the University of Wisconsin–Madison CIMSS Satellite Consensus Intensity Estimates (SATCON; Herndon et al. 2010)], scatterometer data, and subjective guidance from microwave imagery. Surface observations are occasionally used to refine storm intensity. They come from drifting or moored buoys, land-based weather stations, the weather radars of La Réunion, or the 2007 Aeroclipper campaign (Duvel et al. 2009). A reanalysis project is being undertaken by RSMC La Réunion, similar to what was done for the northwestern Australian basin (Harper et al. 2008) and the northern Indian Ocean (Hoarau et al. 2012), specifically for system intensity. This ongoing effort mainly focuses on the period prior to 1998, when there was no Meteosat geostationary satellite directly covering the Indian Ocean. It relies on the hurricane satellite (HURSAT) database, which includes digital imagery from the National Atmospheric and Oceanic Administration (NOAA) polar-orbiting satellites, geostationary imagery from the Meteosat and Geostationary Meteorological Satellite systems, and passive microwave imagery from the Defense Meteorological Satellite Program satellites available since 1987. Within a few years, the reanalyzed database will include systems that formed since 1979. Until then, we will investigate here the 17-yr geostationary-satellite era (1999–2016) that is considered to be homogeneous at the present time.

Previous studies have examined the climatological characteristics of rapid intensification (RI) in the NA (e.g., Lee et al. 2015; Kaplan and DeMaria 2003, hereinafter KD03; Kaplan et al. 2010, hereinafter KD10) and eastern North Pacific Ocean (ENP) (KD10)—two basins that benefit from routine or occasional aircraft reconnaissance. A threshold that is based on the 94th or 95th percentile of the 24-h intensity change was generally employed to define the RI of tropical systems. An increase of $15.4\,\mathrm{m\,s^{-1}\,day^{-1}}$ (30 kt) in the maximum surface winds sustained over 1 min was obtained for rapidly intensifying Atlantic systems, from the National Hurricane Center best-track data (HURDAT) over the 1989–2000 (KD03) or 1989–2006 (KD10) periods. Other thresholds for RI exist in the literature: $18.0\,\mathrm{m\,s^{-1}\,day^{-1}}$ (maximum 1-min sustained wind speed) for ENP systems over the 1989–2006 period (KD10), $12.9\,\mathrm{m\,s^{-1}\,day^{-1}}$ (10-min average wind speed) for western North Pacific (WNP) systems over the 2000–11 period from the final best-track dataset of RSMC Tokyo (Gao et al. 2016), or a minimum drop of $42\,\mathrm{hPa\,day^{-1}}$ in the central sea level pressure as based on 79 intense tropical systems that occurred between 1956 and 1976 over the WNP (Holliday and Thompson 1979). Conditions conducive to rapid decay (RD) were explored over the ENP basin by Wood and Ritchie (2014) who arbitrarily defined RD as a weakening of at least $15.4\,\mathrm{m\,s^{-1}}$ in 24 h. Wang et al. (2015) also used the −30-kt threshold to define rapid weakening in their statistical analysis of the effects of vertical wind shear on tropical-system intensity change over the WNP. No statistical study has yet proposed a proper definition for RD. So far, and by default, forecasting and research applications in the SWIO have used the characteristics and thresholds derived for the NA basin (KD03; KD10).

Despite much effort spent over the last decade in research and operational modeling perspectives, intensification processes are not yet sufficiently understood to allow improvements in intensity forecasts to equal those in track forecasts at 24–72-h lead time (DeMaria et al. 2014). To offer further guidance for practical intensity forecasts over the SWIO and to better anticipate rapid changes in intensity, a future companion study will focus on identifying the dominant large-scale factors that govern the intensity changes of tropical systems. The goal is to deliver a statistical–dynamical tool to predict intensity and/or the probability of RI at short range of the same ilk as those developed for other basins (e.g., DeMaria and Kaplan 1994a; Knaff et al. 2005; KD10; Gao and Chiu 2012).

A key prerequisite, and the objective of this first study, is to provide a description of the climatological behavior (hereinafter referred to as a "climatology") of tropical systems and their rapid changes in intensity in the SWIO. A proper threshold for RI will be defined at the 95% level of 24-h intensity change to follow the method used for Atlantic systems (KD03; KD10) and to enable basin intercomparisons. Likewise, the 5% level of the whole spectrum of intensity change will be used to define RD. Also unknown in the SWIO basin is the statistical relationship linking the observed maximum intensity of a tropical system to the sea surface temperature (SST). Physical reasoning and previous research both suggest an enhanced potential for systems with intensities that are farther from their maximum

potential intensity (MPI) to undergo RI. The MPI that a tropical system can reach under some given atmospheric and oceanic conditions can be obtained theoretically (e.g., Emanuel 1988; Holland 1997); it can also be derived empirically by using BT estimates of the maximum wind speed and SST analyses. The empirical MPI–SST relationship can be exponential, as it is in the NA (e.g., DeMaria and Kaplan 1994b; Zeng et al. 2008) or WNP (Zeng et al. 2007; Gao et al. 2016). It can also be (nearly) linear, as it is in the ENP (e.g., Whitney and Hobgood 1997) or the Bay of Bengal (Kotal et al. 2009). Ng et al. (2016) recently showed that there is not a uniform relationship linking SST to MPI for the entire globe. Over the SWIO basin, the MPI–SST relationship will be derived on the basis of BT data and the most recent NOAA daily Optimum Interpolation SST (OISST; Reynolds et al. 2007) analyses, following the method of Zeng et al. (2007) or DeMaria and Kaplan (1994b).

Another objective of this study is to provide a climatology of tropical-system size in the SWIO and to define very small tropical systems known as midget systems. The most common metrics to measure storm size include the radius of gale-force wind (R34) and the radius of the outermost closed isobar (ROCI), and the inner-core size is generally characterized by the radius of maximum wind (RMW). In the literature, there is no consensus definition for a midget system. The American Meteorological Society glossary (Glickman 2000) defines it as "a tropical cyclone with a radius to the outermost closed isobar of 100–200 km" (http://glossary.ametsoc.org/wiki/Midget_tropical_cyclone), whereas, at the time of writing, Wikipedia defined it as having an ROCI threshold of 2° latitude or 222 km (https://en.wikipedia.org/wiki/Tropical_cyclone). In Fitzpatrick (2005), a system is considered to be a midget system if its R34 is smaller than 65 km (40 mi). To our knowledge, none of these definitions are supported by a systematic analysis. This is probably because a lack of accurate measurements from observations means that there are still some large uncertainties in the estimates of structure parameters, particularly for weak storms. Merrill (1984) studied the climatology of tropical-system sizes in the WNP and NA basins. He found that the ROCI of the "mean" Pacific tropical system was about 1.5° larger than that of the mean Atlantic system but did not attempt to give a statistical definition for small systems. Although there has been limited research on this class of small storms (e.g., Harr et al. 1996), they can be a challenge for intensity prediction because they seem to be highly responsive to their environment (in particular, at high levels), at least in the SWIO. When discussing some of the phenomena that seemed to be problematic for the use of Dvorak's technique, Lander (2004, p. 2) noted that the intensities of midget systems are "often underestimated (especially in the early stages)." Also, Weatherford and Gray (1988a,b) indicated an increased rate of intensification with smaller-sized tropical systems. Satellite observations (Chavas and Emanuel 2010) indicate that the size of a system is only weakly correlated with its intensity. Therefore, it is not because a system is small that it is weak, and recent examples proved it in the SWIO basin [e.g., Fantala (2016) and Hellen (2014) are considered to be the most intense systems ever recorded in the basin]. The quantitative analysis of best-track sizes in the SWIO will be a first attempt toward a statistical definition of midget systems in the SWIO.

Section 2 describes the datasets and terminology used for the statistical analysis of SWIO tropical systems. Section 3 presents a climatology of tropical systems, their tracks, landfall or near-landfall frequency on coastal areas, monthly distribution, and sizes. A statistical definition for a midget system is then derived. Section 4 offers a formulation of the empirical MPI in the basin. The 24-h intensity changes (intensification or decay) are examined in section 5, and thresholds are derived for RI and RD in the SWIO basin. Section 6 gives a summary and outlines possible future investigations.

2. Data and analysis

In this study, we examine the final analysis of BT data produced by RSMC La Réunion. We focus on the currently most reliable 17-yr period of the geostationary-satellite era encompassing the 1999/2000–2015/16 cyclone seasons. The database includes 6-hourly estimates of storm location (latitude–longitude), Dvorak current intensity (CI), maximum 10-m wind speed (VMAX), central sea level pressure, motion (speed and heading) computed from storm positions, and different size parameters (ROCI, R34, and RMW). The World Meteorological Organization (WMO) standard 10-min average is used to define the maximum wind speed. Considering that the Dvorak scale has been traditionally assumed to be for a 1-min sustained wind (Velden et al. 2006), forecasters employ an empirical 0.88 factor (WMO 2017) to convert the 1-min sustained estimate of peak storm intensity deduced from the Dvorak-related intensity estimate CI. The BT intensity estimates are usually provided to the nearest 5-kt interval (or 2.6 $m\,s^{-1}$), but occasional BT fixes have values within the nearest 2- or 3-kt interval. Because knots are the native unit for estimating storm intensity with the Dvorak technique, they will be used for storm categorization and wind bins in the remainder of the paper (1 kt = 0.514 $m\,s^{-1}$).

The SWIO basin has a specific terminology for tropical-system classification. Unlike most basins in

which all systems are labeled as tropical cyclones (TC) regardless of intensity, the term ''tropical cyclone'' is reserved to describe systems with 10-min average maximum wind speeds of greater than or equal to 64 kt (VMAX $\geq$ 32.9 m s^{-1}). The generic term ''tropical disturbance'' is used for a nonfrontal area of low pressure that has organized convection and a definite cyclonic surface wind circulation, with maximum surface winds of less than or equal to 27 kt (13.9 m s^{-1}). Beyond that threshold, the system is designated as a tropical depression. In the current study, tropical disturbances and tropical depressions will be grouped under the same term TD (VMAX $<$ 34 kt or 17.4 m s^{-1}) to enable basin intercomparisons (there is no minimum intensity threshold in the official definition of a TD in other basins). When VMAX reaches or exceeds 34 kt, the system is assigned a name and is classified as a moderate tropical storm (TS). The ensuing stages of intensification are severe tropical storm (VMAX $\geq$ 48 kt or 24.6 m s^{-1}), tropical cyclone (VMAX $\geq$ 64 kt or 32.9 m s^{-1}), intense tropical cyclone (VMAX $\geq$ 90 kt or 46.3 m s^{-1}), and very intense tropical cyclone (VMAX $\geq$ 116 kt or 59.6 m s^{-1}).

In this study, we consider storms that reached at least the tropical disturbance stage, which excludes disturbed weather zones with unorganized convection. This results in 165 such tropical systems associated with 4869 cases that contain a maximum wind speed estimation in the BT dataset. This sample is used at the beginning of section 3 to study the tracks of tropical systems in the SWIO and to quantify how exposed the various countries of the region are. For the rest of the study, the data are then restricted to periods during which storm centers are over water and storms are tropical: ''extratropical,'' ''post tropical,'' and ''subtropical'' systems are excluded in the sampled cases, as in KD03. This ensures the legitimate use of the Dvorak technique and enables basin intercomparisons. The maximum wind is used to diagnose storm intensity. The methods are the same as employed in KD03 and KD10, and the following sentence is derived from those sources with minor modifications: Intensification or weakening periods are evaluated at the beginning (t = 0 h) of each 24-h interval in the database, provided that the system remains over water during the period from t − 12 to t + 24 h. The BT dataset contains 165 overwater tropical systems associated with 4833 observations of VMAX, of which 4401 observations from 164 systems can be used to compute changes in storm intensity over 24-h lags.

The MPI–SST relationship is derived using 0.25° daily OISST data (Reynolds et al. 2007) provided by the NOAA/OAR/ESRL Physical Sciences Division (http://www.esrl.noaa.gov/psd/). For the current study, SST values were extracted at each storm-center location using linear time interpolation and bilinear spatial interpolation. Sea surface temperatures from the global European Centre for Medium-Range Weather Forecasts interim reanalysis (ERA-Interim, hereinafter shortened to EI; Dee et al. 2011) are also retrieved at 6-h intervals (no time interpolation needed) and T255 (0.75° latitude–longitude) resolution to see whether and how the SST dataset affects the MPI–SST relationship.

3. Climatology of system tracks, impacts, activity, seasonal variations, and sizes

This section first reports on the tracks of tropical systems in the SWIO and how frequently the countries of the region are exposed to storm hazards. Then, the climatology of overwater tropical systems (number of systems in each category; monthly distributions) is described. A quantitative analysis of the different sizes of SWIO storms is finally performed to provide a statistical definition for midget systems.

a. Tracks

Tropical systems are uniformly distributed over the basin from 35° to 95°E (Fig. 1). They mainly move southwestward, in accordance with the prevailing environmental steering (easterly trade winds) and with the beta effect (Holland 1983; Chan and Williams 1987), before they recurve southward or southeastward for their extratropical transition. Over the open Indian Ocean, TCs that are equivalent in intensity to a hurricane or typhoon are mostly confined to the 10°–25°S latitude band, north of the gradient of cool-to-colder SSTs (Fig. 2). In the Mozambique Channel, however, the activity shifts approximately 5° southward and TCs occur more frequently between 15° and 30°S. This shift is mainly due to a farther-poleward position of the monsoon trough (which spawns most SWIO storms) and to higher SSTs at these latitudes relative to those in the open ocean (Fig. 2).

b. Coastal hits and threats

Table 1 lists the number of distinct tropical systems classified as TDs, TSs, or TCs that hit or threatened each of the SWIO basin countries mapped out in Fig. 1. Only the coastal areas are considered here, which excludes the two cases of Dando (2012) and Eline (2000) (Reason and Keibel 2004) that penetrated into South Africa after making landfall on the Mozambique coast. Counted as threatening events are storms whose center skirted the coast of a given territory or island within less than 100 km without making landfall; their intensity was taken at the point of closest approach from land. Any storm hitting an island (e.g., Madagascar) several times

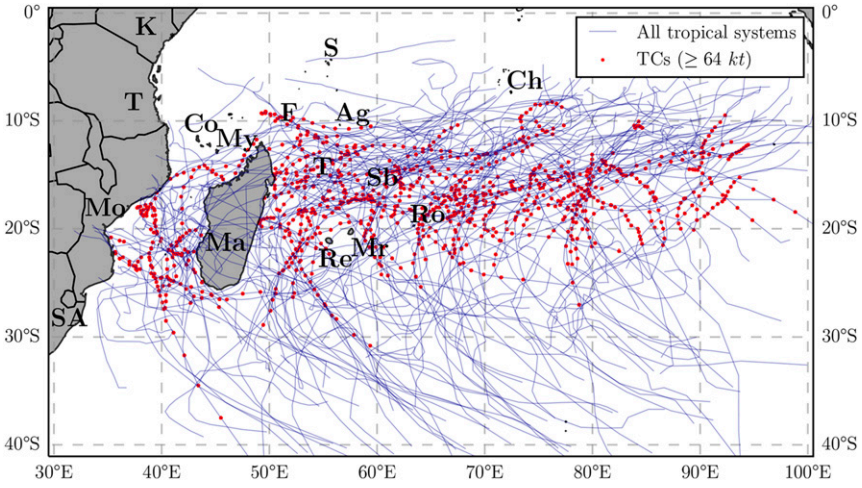

FIG. 1. Tracks of all SWIO tropical systems with a VMAX observation in the BT dataset during the 1999–2016 period. Red colors indicate that a system has reached TC intensity over water (VMAX ≥ 64 kt or 32.9 m s^{-1}). Letters SA, Mo, T, and K indicate South Africa, Mozambique, Tanzania, and Kenya, respectively. Letters Co, My, Ma, F, T, S, Re, Mr, Ag, Sb, Ro, and Ch indicate the islands of Comoros, Mayotte, Madagascar, Farquhar, Tromelin, Seychelles, La Réunion, Mauritius, Agalega, Saint Brandon, Rodrigues, and the Chagos Archipelago, respectively. Some islands or atolls are too small for their borders to be seen in the map. The total sample size is 4869.

is only counted once in Table 1 and is classified according to the maximum landfall intensity.

Table 1 shows that many countries in the SWIO are affected by tropical systems on a regular basis. Mozambique, located on the eastern coast of Africa and bordered in the north by Tanzania and in the south by South Africa, was hit by tropical systems once per year, on average, and by TCs about once every 3 years over the period encompassing the 1999/2000–2015/16 cyclone seasons. Those numbers double for Madagascar, the fourth-biggest island on Earth and one of the poorest countries in the world: it was hit twice and threatened once per year by tropical systems and was hit once every 2 years and threatened once every 4 years by TCs, mostly on its eastern coast. Neither the Kenyan nor the South African coasts were impacted by tropical systems. Forming 40 km off the coast of Tanzania was TC Hellen (2014). Owing to their much smaller sizes, the twin

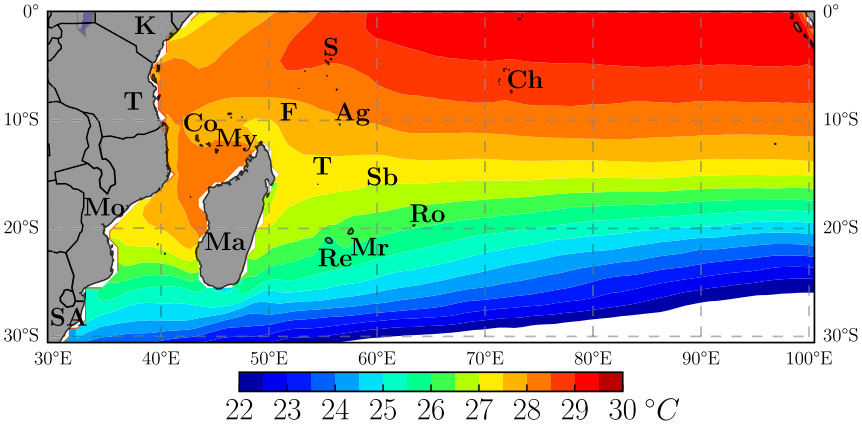

FIG. 2. Climatology of mean SSTs exceeding 22°C in the meridional part of the SWIO basin for the active cyclone seasons from September to June during the 1999–2016 period. Temperatures are extracted from the 6-h-resolution global EI dataset at 0.75° latitude–longitude resolution (Dee et al. 2011). Letters indicate the various islands or countries as in Fig. 1. The total sample size is 170 months.

TABLE 1. Number of tropical systems that hit or threatened the coast of each Indian Ocean territory (listed in increasing order of latitude) during the 1999–2016 period. "Direct hit" means that the storm center made landfall; "threat" means that the storm center was located on the sea less than 100 km from the coast. The system categories (intensity classes) at the time of landfall or of closest approach are indicated in the columns, with the corresponding VMAX (kt). The total numbers N of systems classified in each category according to their lifetime maximum intensity over the 17-yr period are given in the header row.

	TD (VMAX < 34; N = 6)		TS (34 ≤ VMAX < 64; N = 77)		TC (VMAX ≥ 64; N = 82)		All systems (N = 165)	
	Direct hits	Threats	Direct hits	Threats	Direct hits	Threats	Direct hits	Threats
South Africa	0	0	0	0	0	0	0	0
Mozambique	9	15	2	1	5	5	16	21
Tanzania	0	1	0	0	0	0	0	1
Kenya	0	0	0	0	0	0	0	0
The Comoros archipelago	1	0	0	3	0	0	1	3
Mayotte archipelago	0	1	1	2	0	0	1	3
Madagascar and islands	11	11	13	3	10	4	34	18
Farquhar Atoll	1	5	0	0	0	2	1	7
Tromelin	0	8	1	6	0	2	1	16
Seychelles archipelago	0	0	0	1	0	0	0	1
La Réunion	1	2	0	1	0	3	1	6
Agalega archipelago	0	4	0	3	0	2	0	9
Mauritius archipelago	0	2	0	3	0	2	0	7
Saint Brandon archipelago	2	8	1	9	1	5	4	22
Rodrigues archipelago	1	3	1	4	0	3	2	10
Chagos Archipelago	0	2	0	0	0	0	0	2

islands La Réunion and Mauritius only suffered from seven systems during the 17-yr period, but two-thirds of them were at or above the TS stage. The Chagos Archipelago—located around 6°S, 72°E—is in an area where many depressions form (Fig. 1).

c. *Overwater tropical-systems climatology*

During the 1999–2016 period, 165 tropical systems were observed over water in the SWIO (Table 1); 96% of them reached the tropical-storm stage (defined by VMAX ≥ 34 kt), and 50% of them reached the tropical-cyclone stage (defined by VMAX ≥ 64 kt). Among the 82 TCs, 41 became intense (90 ≤ VMAX < 116 kt) and 14 became very intense (VMAX ≥ 116 kt). Thus, 9.7 tropical systems develop in the SWIO basin on average each year, of which 9.4 are named as they strengthen into tropical storms and 4.8 go on to become TCs that are equivalent to a hurricane or a typhoon. This represents about 11% of global tropical-system activity and is almost equal to the activity in the North Atlantic (WMO 2017).

The official cyclone season runs between 1 July and 30 June in the SWIO, but the basin only experienced activity from September to June during the 1999–2016 period (Fig. 3a). Note that Abela, the first system of the latest 2016/17 season that is not included in this 17-yr climatology, was the first SWIO event to form in July since 1999, and it reached the stage of severe tropical storm (defined by VMAX ≥ 48 kt). Figures 3a and 3d also show that more than 74% of tropical systems and 81% of TCs are observed during the warm and wet season that spans from December to March, when the ocean is warmer.

d. *Storm size and midget systems*

Storm size can be measured by the radius of gale-force wind or by the radius of the outermost closed isobar, while a common scale for vortex size is the radius of maximum wind. The ROCI parameter is found 3011 times in the BT dataset for 160 overwater tropical systems. Over the 1999–2016 period, the ROCI ranges from 55 to 1110 km (10°), with a mean of 405 km. A total of 303 observations (10%) have an ROCI of less than the 2°-latitude (222 km) threshold found in the literature. Using the fifth percentile of storm size distribution, a midget system in the SWIO could be defined as a system with an ROCI that is lower than or equal to 197 km. The quality and homogeneity of the ROCI dataset over the period are uncertain, however.

A more robust dataset is the radial extent of the 34-kt wind. The R34 parameter started to be estimated by the La Réunion center and recorded by quadrants in the best track at the beginning of the 2010/11 cyclone season. There are 817 observations available after computing averages over the four quadrants of each storm. The R34 parameter ranges from 15 to 430 km, with a mean of 152 km. A total of 115 observations (14%) have an R34 that is less than the 65-km threshold found in the literature. Using the fifth percentile of storm size distribution, a midget system in the SWIO can be

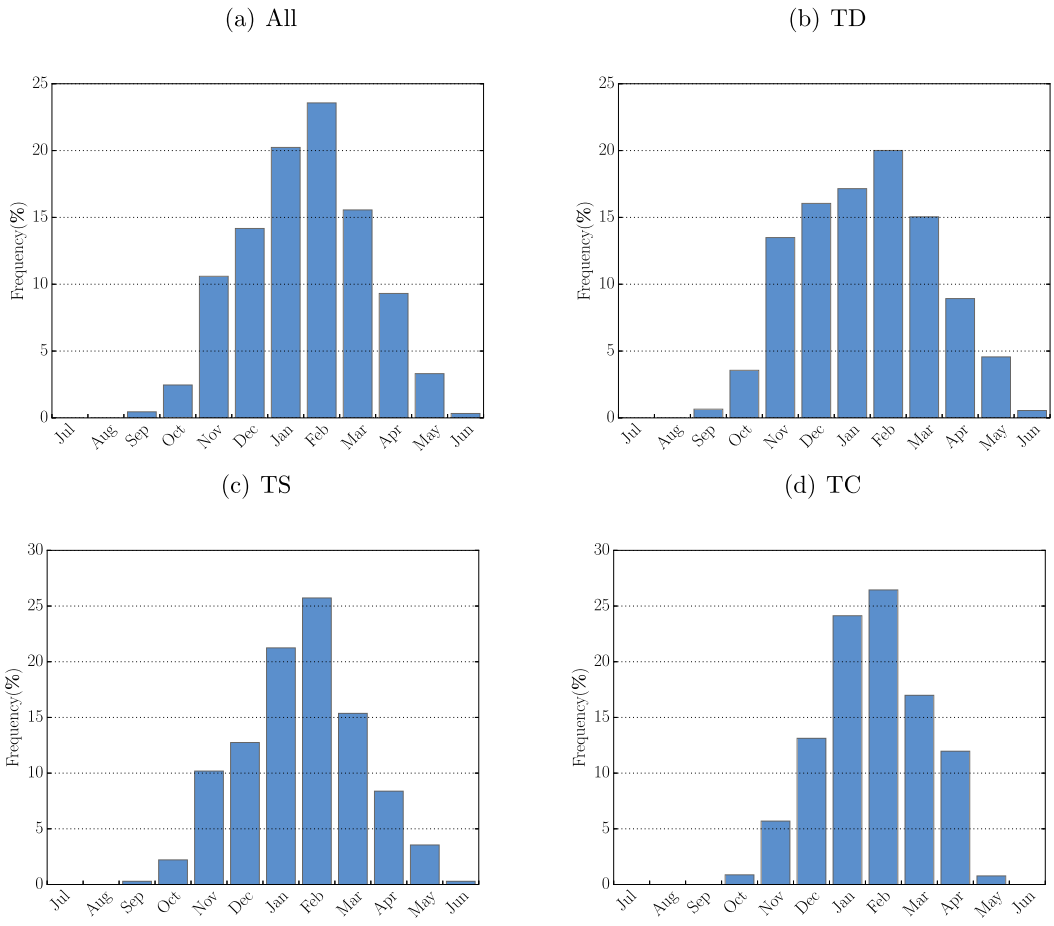

FIG. 3. Monthly distributions of overwater tropical-system cases stratified by storm intensity at time $t = 0$ h during the 1999–2016 period. The abscissa spans the 12 months. The ordinate shows frequencies for each category of systems—(a) all, (b) TDs, with VMAX $<$ 34 kt, (c) TSs, with 34 $\leq$ VMAX $<$ 64 kt, and (d) TCs, with VMAX $\geq$ 64 kt—obtained by dividing the number of cases per month in a given category by the total number of cases in that same category. The total sample size is 4833.

defined as a system with R34 $\leq$ 46 km. With this definition, a total of 21 of 52 systems were midget systems at least once during their lifetime. The nonmidget observations are associated with 51 distinct systems.

Only 24% of observations that are classified as midget cases upon the R34 criterion also verify the first midget criterion (ROCI $\leq$ 197 km). This is due in part to the natural variability of storm sizes but also most likely to the uncertainty in the ROCI estimation. A one-sided test that assumes unequal sample variances (the Welch t test) is used to investigate whether statistically significant differences exist at the 95% confidence level between the means of the midget and nonmidget system samples defined by the R34 criteria. Distinct variables are tested: the latitude, longitude, storm speed and heading, maximum wind, radius of maximum wind, and 24-h intensity change computed for a maximum of 806 observations (Table 2). Both the maximum winds and the radius of maximum winds (available for a subset of 727 observations) are statistically significantly different. Midget systems are, on average, significantly weaker (21.1 m s^{-1}) than the rest of the sample (33.4 m s^{-1}), possibly reflecting the frequent Dvorak underestimation of their intensity, as noted by Lander (2004). Their mean inner-core extension, defined by the radius of maximum wind, is much smaller (34 km) than that of the rest of the sample (46 km), which is consistent with both their mean smaller R34 extension (36 vs 160 km) and mean smaller ROCI extension (310 vs 395 km). Their mean 24-h wind speed change is also significantly higher (3.8 m s^{-1}) than that of the rest of the sample (-1.0 m s^{-1}). They experience significantly more intensification periods (an increase of the maximum wind over 24 h) and fewer decay periods than nonmidget systems (Z test for two population proportions; Table 3). Samples for midget and nonmidget systems defined by the R34 criteria are

TABLE 2. Statistics related to midget and nonmidget events from the six cyclone seasons (2010/11–2015/16) for which the R34 parameter was recorded; events are classified on the basis of an R34 threshold of 46 km. The *N* gives sample size. Highlighted in boldface are values that are significantly different in the two samples at the 95% level. Shown here are the mean values of several BT parameters and their statistical significance using a Welch's one-sided *t* test.

			Midget		Nonmidget	
Variable	Definition	Units	Mean	*N*	Mean	*N*
R34	Radius of gale-force wind (34 kt)	km	**35.9**	43	**159.6**	763
LAT	Storm-center latitude	°N	−16.3	43	−17.6	763
LON	Storm-center longitude	°E	63.2	43	65.6	763
HDG	Storm-motion heading	°	201.7	43	188.1	763
SPD	Storm-motion speed	$m\,s^{-1}$	3.8	43	4.2	763
VMAX	Max 10-min mean wind speed	$m\,s^{-1}$	**21.1**	34	**33.4**	693
Rmax	Radius of max wind	km	**34.3**	34	**46.2**	693
ROCI	Radius of the outermost closed isobar	km	**310**	42	**395**	700
ΔV_{24}	24-h wind speed change	$m\,s^{-1}$	**3.8**	43	**−1.0**	763
$\Delta V_{24} > 0$	Positive 24-h wind speed change	$m\,s^{-1}$	10.5	43	9.5	763
$\Delta V_{24} \leq 0$	Negative 24-h wind speed change	$m\,s^{-1}$	−6.6	43	−7.9	763

unfortunately too small beyond a 6-h lead time to allow running of standard *t* statistics on operational forecast errors and to determine whether midget systems represent a challenge for intensity or track prediction, but it seems so when statistics are conducted over the less-reliable ROCI criteria (not shown). With a larger dataset in the future, statistics could also be run with a restriction on the initial intensity of all systems to screen out developing tropical systems that are yet to grow, both in size and in intensity; a 48-kt-or-greater threshold would help to distinguish developing systems from mature midgets. Weak systems of small size may cloud the current statistics and may explain, in part, why the midget sample has a lower mean intensity than the comparison group.

4. Climatology of storm maximum intensity

a. Empirical maximum potential intensity

As shown in section 3, westward-tracking systems often hit Madagascar; the ones that survive the long island trip emerge weak over particularly warm waters exceeding 29.5°C in the Mozambique Channel (Fig. 2). To work on a sample with homogeneous characteristics, systems are therefore filtered out after making landfall on Madagascar. An exception is made for the eight systems that managed to reintensify over the Mozambique Channel as a result of its particularly warm waters exceeding 29.5°C (Fig. 2), because the behavior of these residual vortices follows that of cyclogenesis in the channel. A total of 4164 cases are thus extracted from the database to analyze the distribution of maximum intensity versus SST in the SWIO basin (Fig. 4).

Following DeMaria and Kaplan (1994b), ocean observations are extracted under each storm center and divided into 1°C intervals (Table 4). They range from 21.9° to 31.0°C. There are too few observations exceeding 30.5°C to include the 31°C-midpoint group in the following analysis. Note that, unlike DeMaria and Kaplan (1994b) and subsequent empirical MPI formulations, wind speeds are not evaluated in storm-relative coordinates. DeMaria and Kaplan (1994b) decided to subtract the storm translational speed from the maximum wind estimate to follow a comment made by

TABLE 3. Statistics related to midget and nonmidget events from the six cyclone seasons (2010/11–2015/16) for which the R34 parameter was recorded; events are classified on the basis of an R34 threshold of 46 km. The *N* gives sample size. Highlighted in boldface are values that are significantly different in the two samples at the 95% level. Shown here are the number of events for different thresholds of 24-h intensity change (ΔV_{24};, $m\,s^{-1}$) and their statistical significance using a *Z* test to compare two population proportions.

Variable	Definition	Midget (N = 43)	Nonmidget (N = 763)
$N_{\Delta V_{24}>0}$	Events with $\Delta V_{24} > 0$ (intensification)	**26**	**303**
$N_{\Delta V_{24}\leq 0}$	Events with $\Delta V_{24} \leq 0$ (maintaining or weakening)	**17**	**460**
$N_{\Delta V_{24}\geq 15.4}$	Events with $\Delta V_{24} \geq 15.4\,m\,s^{-1}$ (RI)	8	70
$N_{\Delta V_{24}<15.4}$	Events with $\Delta V_{24} < 15.4\,m\,s^{-1}$ (non RI)	35	693
$N_{\Delta V_{24}\leq -13.9}$	Events with $\Delta V_{24} \leq -13.9\,m\,s^{-1}$ (RD)	2	82
$N_{\Delta V_{24}>-13.9}$	Events with $\Delta V_{24} > -13.9\,m\,s^{-1}$ (non RD)	41	681

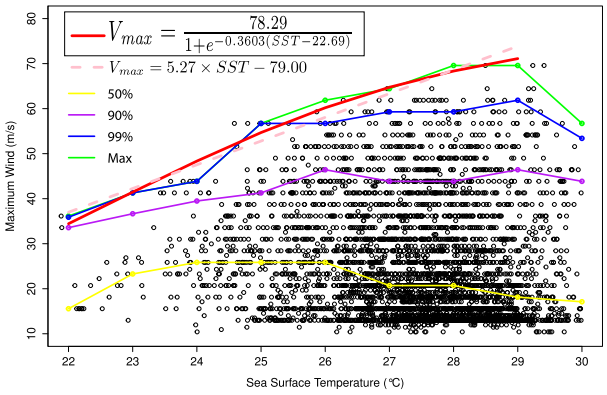

FIG. 4. Scatter diagram of maximum wind speed ($m\,s^{-1}$) vs SSTs (°C) at storm locations during the 1999–2016 period. The SSTs were interpolated from the OISST dataset. The green, blue, purple, and yellow lines respectively show the observed maximum intensity and the 99th, 90th, and 50th intensity percentiles for each 1°C SST bin. The red least squares curve is fitted to the binned maximum intensity in the 22°–29° SST range and gives the empirical MPI formulation. The dashed pink line shows the linear fit obtained over the same SST range. The total sample size is 4164.

Merrill (1987, p. 10) on the SST capping function: "A smoother relationship results if relative intensities are used, since many of the extreme wind speeds found at high latitudes were associated with rapidly moving storms." Merrill (1987) was actually discussing extratropical-transition systems for which the strongest winds had moved out and away from the center and were more in line with the faster movement of the storm. As detailed in section 2, extratropical, subtropical, and post-tropical cases were filtered out in our sample, which is reflected by a higher minimum SST bin value of 22°C versus 12° or 15°C for Merrill (1987) and DeMaria and Kaplan (1994b), respectively. Subtracting the forward motion of the tropical cyclone from the best-track intensity is therefore unnecessary and would only create a bias toward slower-moving systems. As pointed out by Courtney and Knaff (2009, p. 174) "reducing the Dvorak-derived maximum wind to a storm-relative value prior to calculation ignores the fact that there is a mean TC motion implicit in the technique." The mean translational speed of the sample is 7.8 kt ($4.0\,m\,s^{-1}$) versus $6\,m\,s^{-1}$ of that in DeMaria and Kaplan (1994b) for NA storms. The only six records in the sample for which the storm speed exceeds 25 kt ($12.9\,m\,s^{-1}$) are related to five distinct tropical systems at the early stage of their extratropicalization, 6 or 12 h before they were eventually classified as extratropical.

The maximum wind and the 99th percentile exhibit a decreasing trend for SSTs above 29.0°C. This result is different from the mere flattening (but still increasing) slope found by DeMaria and Kaplan (1994b) above 28.0°C in the NA but is more similar to the flattening or decrease found by Gao and Chiu (2012) in the WNP beyond 28.5°C. It reflects the unique features of the Mozambique Channel, which spawns systems over very warm waters but offers them very little room and time for intensification before landfall. For that reason, the empirical MPI function was derived with an SST cutoff of 29°C. The shape of the maximum and 99th-percentile curves suggested an exponential-like fit to SST observations (Fig. 4, red curve) of the form

$$\mathrm{MPI} = \frac{A}{1 + e^{-B(\mathrm{SST}-T_0)}}, \tag{1}$$

with SST within the 22°–29°C range. Using a least squares fit, the resulting coefficients are given by $A = 78.29\,m\,s^{-1}$, $B = 0.3603°C^{-1}$, and $T_0 = 22.69°C$. The average error between the computed MPI (Fig. 4, red curve) and the maximum wind (green curve) is $1.6\,m\,s^{-1}$ over the eight SST bins ranging from 22° to 29°C.

This exponential function differs from the positive exponential fit

$$\mathrm{MPI} = A' + B' e^{C'(\mathrm{SST}-T_0')}$$

obtained in the NA (e.g., DeMaria and Kaplan 1994b; Zeng et al. 2008) and WNP (Zeng et al. 2007; Gao et al. 2016). The use of the linear relationship MPI = $D \times$ SST + E, with $D = 5.27°C^{-1}$ and $E = -79.00\,m\,s^{-1}$ (dashed pink line in Fig. 4), yields an average error of $2.45\,m\,s^{-1}$ over the eight SST bins.

To test the sensitivity of the MPI–SST relationship to the SST dataset, EI ocean temperatures are also examined. They vary between 21.0° and 30.7°C over the study period. A positive exponential fit

$$\mathrm{MPI} = A' + B' e^{C'(\mathrm{SST}-T_0')}$$

is obtained within the same 22°–29°C range with the following coefficients: $A' = 9.53\,m\,s^{-1}$, $B' = 70.63\,m\,s^{-1}$,

TABLE 4. Observations of maximum winds and SSTs stratified into nine 1°C bins during the 1999–2016 period. The SSTs were interpolated from the OISST dataset (Reynolds et al. 2007).

SST midpoint (°C)	No. obs	Avg SST (°C)	Avg intensity ($m\,s^{-1}$)
22.0	11	22.2	20.5
23.0	17	23.0	24.6
24.0	98	24.1	26.8
25.0	256	25.1	26.5
26.0	507	26.1	28.5
27.0	1085	27.1	24.9
28.0	1358	28.0	24.6
29.0	691	28.9	23.6
30.0	130	29.8	22.9

$C' = 0.1319°C^{-1}$, and $T_0' = 30.0°C$. The mean error is $2.8\,m\,s^{-1}$ over the eight SST bins. The differences between the two MPI relationships (using OISST or EI SST data) take the form of a concave curve over the 22°–29°C interval, with a mean of $5.1\,m\,s^{-1}$ and a maximum of $8.9\,m\,s^{-1}$. Correcting EI SSTs with a −1°C bias yields a similar fit to that obtained for the OISST data [Eq. (1)] and a considerable reduction in differences between MPI formulas (mean $1.1\,m\,s^{-1}$; maximum $2.0\,m\,s^{-1}$). The OISST data are finally chosen over the EI SST data in the SWIO basin for several reasons: 1) most empirical MPI formulas worldwide have been derived from the OISST dataset, 2) the OISST dataset has a finer resolution, 3) the average difference between the computed MPI and the maximum wind in the BT dataset is minimized, and 4) the OISST dataset is the one that is currently available to La Réunion forecasters for operations.

b. *Relationship between SST and tropopause temperature*

If one takes the temperature at 100 hPa as a rough proxy for the tropopause temperature, which provides a lower-bound estimate of the temperature T_{out} in the outflow layer of the storm, Fig. 5a shows that the outflow temperature is strongly controlled by the SST (overall negative correlation). In Emanuel's theory, the outflow temperature controls the theoretical maximum wind speed (Bister and Emanuel 1998) via the thermodynamic efficiency ε of the ideal Carnot heat engine:

$$\varepsilon = \left(\frac{\mathrm{SST} - T_{out}}{T_{out}}\right)^{1/2}. \qquad (2)$$

Figure 5b confirms that ε is approximately a linear function of SST, as previously noticed by Zeng et al. (2007) in the WNP and Zeng et al. (2008) in the NA. This proves that, to a first approximation (assuming a uniform ambient relative humidity), the maximum intensity is a function only of SST as argued by Emanuel (1987) and therefore that the empirical MPI derived in Eq. (1) implicitly includes the effect of the outflow temperature on storm intensity. This conclusion holds when lower levels—such as 150 or 200 hPa—are used to estimate the tropopause temperature; higher outflow layer temperatures only yield a slightly lower mean ε (closer to 0.6). The empirical MPI also implicitly includes the other factors that control storm intensity such as the vertical wind shear [not shown here but highlighted in Zeng et al. (2008)].

c. *Storm relative lifetime peak intensity*

To assess how close a tropical system gets to its empirical MPI, the SST-determined MPI is calculated at the time of the storm's peak intensity using Eq. (1). The relative peak intensity is then defined as the following percentage (Zeng et al. 2007): (VMAX/MPI) × 100%. For the SWIO dataset, the minimum and maximum relative intensities in the sample are 20% and 109%, respectively (not shown). These values are subject to possible errors related to the SST determination at the time of passage or to the Dvorak intensity analysis. The system that exceeded its empirical MPI was in favorable atmospheric environmental conditions. Cyclone Amara's lifetime maximum intensity reached $56.6\,m\,s^{-1}$ (VMAX = 110 kt) in mid-December 2013 over the open ocean near Rodrigues (20°S). The SST was quickly decreasing below 25°C, giving an MPI of $52.0\,m\,s^{-1}$. Storm intensity started

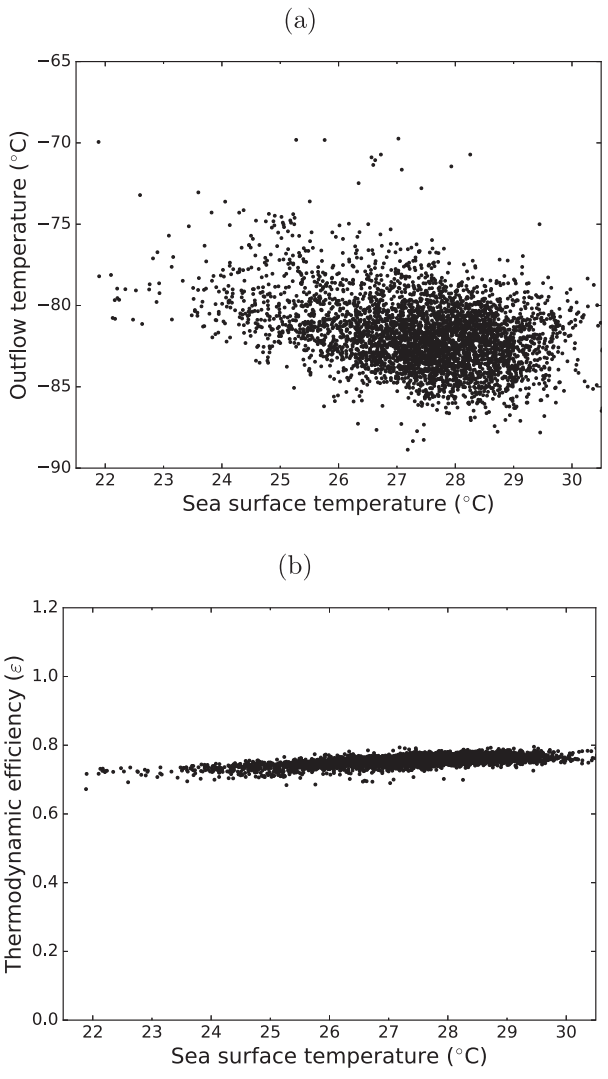

FIG. 5. Scatter diagrams of (a) 100-hPa temperature (°C) from EI (Dee et al. 2011) and (b) the corresponding thermodynamic efficiency ε defined by Eq. (2) vs SST (°C) at storm locations during the 1999–2016 period. The SSTs were interpolated from the OISST dataset. The total sample size is 4164.

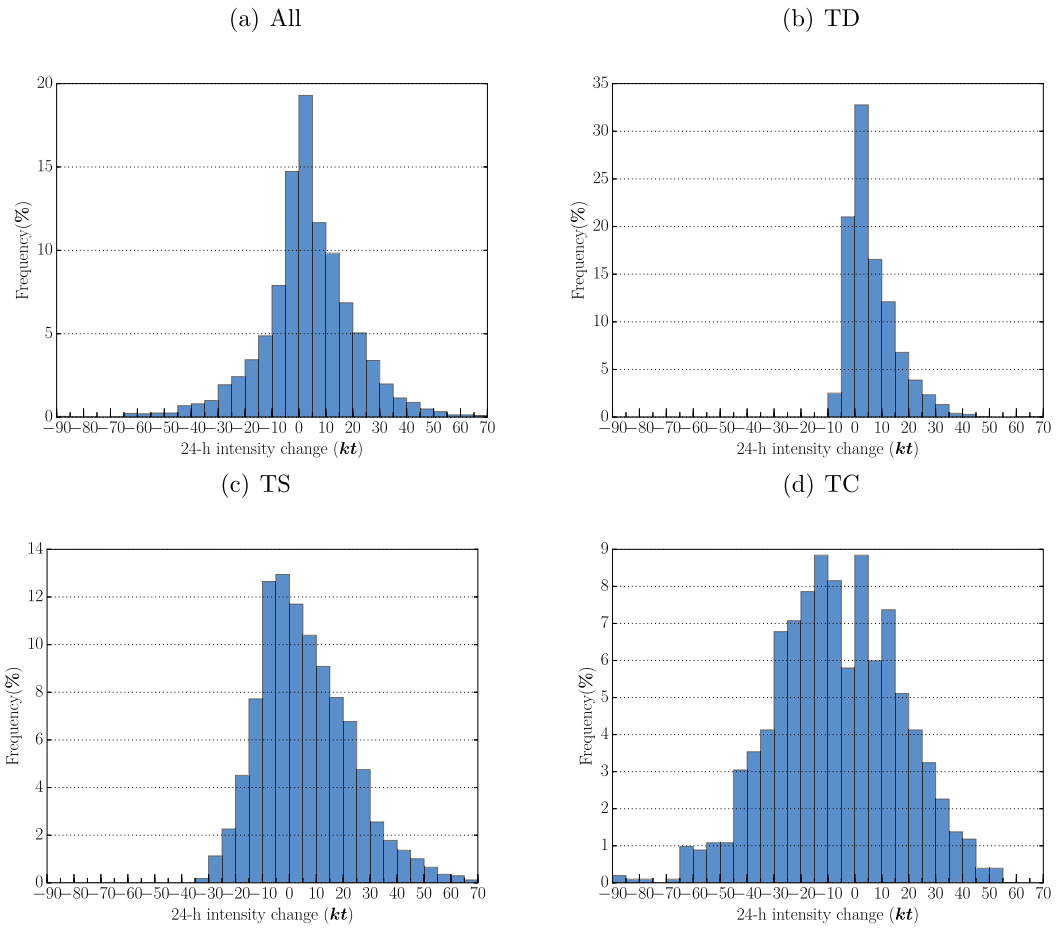

FIG. 6. Frequency distribution of overwater 24-h intensity changes (ΔV_{24}; kt) stratified by storm intensity at time $t = 0$ h during the 1999–2016 period. The ordinate shows frequencies obtained by dividing the number of cases in a given 5-kt interval for a given category by the total number of cases in that category. The total sample size is 4401.

to rapidly weaken 6 h afterward. The MPI was likely exceeded because of the delayed response of storm intensity to reduced SSTs.

The mean relative peak intensity of the sample is 57%, and about 53% and 20% of tropical systems reached 50% and 80%, respectively, of their MPI (not shown). These figures are similar to those obtained by DeMaria and Kaplan (1994b) over the NA (55%, 58%, and 19%, respectively), as well as the distribution of relative peak intensity (not shown; Fig. 6 of DeMaria and Kaplan 1994b). Unfavorable environmental conditions such as vertical shear (e.g., Wang et al. 2015), dry air intrusion from the lower or middle troposphere (Shu et al. 2014; Ge et al. 2013), and SST cooling in the vicinity of the storm (e.g., Vincent et al. 2012) are likely the main reasons why most storms stop intensifying before they reach their MPI. Furthermore, land interactions with Madagascar on the western side of the SWIO basin may prevent many westward-tracking systems from reaching their MPI.

5. Climatology of 24-h storm intensity changes and rapid intensity changes

In this section, the climatology of 24-h storm intensity changes is examined, and a definition of rapid intensification is provided. Climatological characteristics of tropical systems undergoing RI in the SWIO are then highlighted and compared with those found in the NA basin (KD03; KD10). Last, a definition and a climatology for RD events are proposed.

a. 24-h intensity-changes climatology

After computing 24-h intensity-change statistics for overwater tropical systems, the sample is reduced from 165 to 164 systems and from 4833 to 4401 cases. The frequency distribution of ΔV_{24} for all tropical systems (Fig. 6a) indicates that intensity changes in the SWIO are almost normally distributed, with a mean value of 1.1 m s^{-1} (Table 5). The distribution is less skewed toward positive intensity changes in the SWIO than in the

TABLE 5. Overwater 24-h intensity change statistics of the maximum wind speed (ΔV_{24}; m s^{-1}) for all and each category of tropical system (VMAX; kt) during the 1999–2016 period: number of cases N, mean, standard deviation σ, minimum, maximum, range, mean of intensification ($\Delta V_{24} > 0$; m_{int}), and mean of weakening ($\Delta V_{24} < 0$; m_{weak}). Units are meters per second for all parameters but N.

Category	N	Mean	σ	Min	Max	Range	m_{int}	m_{weak}
TD (VMAX < 34 kt)	1808	2.5	4.6	−6.7	32.4	39.1	5.5	−2.2
TS (34 ≤ VMAX < 64 kt)	1629	2.4	8.5	−18.0	35.0	53.0	8.8	−5.5
TC (VMAX ≥ 64 kt)	964	−3.7	11.2	−41.2	25.7	66.9	8.9	−11.5
All	4401	1.1	8.3	−41.2	35.0	76.1	7.3	−6.6

NA basin (KD03; KD10) for several possible reasons. Tropical depressions and storms have a tendency to intensify (Figs. 6b,c) with a mean ΔV_{24} rate of 2.5 and 2.4 m s^{-1}, respectively (Table 5), but this propensity is weaker than in the NA (3.2 and 3.4 m s^{-1}, respectively; Table 2 of KD03). The finding that TDs and TSs have an average lower ΔV_{24} rate in the SWIO than in the NA may be attributable to different oceanic characteristics (narrower continental shelfs on most SWIO coasts) and/or to the impact of dry and dusty Saharan air—with the indirect effects of aerosols—on storm development and intensification in the NA basin (Carlson and Prospero 1972; Dunion and Velden 2004; Braun 2010; Braun et al. 2013; Herbener et al. 2014). If earlier studies following Dunion and Velden (2004) agreed that the Saharan air layer may slow intensification during the predepression-to-depression stages (Braun 2010; Braun et al. 2013), Herbener et al. (2014) showed that the modification of cloud properties via aerosols injected into idealized TCs may initiate interactions between cloud microphysics and storm dynamics that can ultimately lead to a general increase in storm intensity (and a decrease in storm size). Table 5 also indicates that TCs have a strong tendency to weaken, with a significantly higher mean ΔV_{24} rate of −3.7 m s^{-1} than that found in the NA basin (−0.7 m s^{-1}; Table 2 of KD03). This is partly because decay occurs for 60% of TC cases (Fig. 6d), a comparatively higher frequency than that in the NA (about 50%; KD03) and because the maximum decay rate for TCs over water in the 17-yr period of study [−80 kt or −41.2 m s^{-1} per 24 h for TC Hellen (2014) in the Mozambique Channel; Table 5] is significantly greater than the one found in the NA over a 12-yr period (−25.7 m s^{-1} per 24 h; Table 2 of KD03). This could be due to fewer landfalls in the SWIO, increasing the likelihood of capturing most of the life cycle of systems (until their extratropical transition).

Figures 6b and 6c also indicate that 73% of intensity changes in tropical depressions are within a ±10-kt range and that more than 36% of tropical storms have intensity changes of greater than +10 kt. This result suggests that the more organized a tropical system is, the more it is prone to rapid intensity changes: both the standard deviation and range of ΔV_{24} increase with storm intensity class (Table 5). The absolute mean 24-h intensification and weakening rates are larger for TCs, but the maximum 24-h intensification and weakening rates are observed for tropical storms and cyclones, respectively, with a +35 and −41.2 m s^{-1}, respectively, ΔV_{24} value (Table 5). As explained by KD03, this results from the fact that TSs are farther away from their MPI than TCs are and, thus, have more potential to intensify faster. Also, a tropical depression is not yet sufficiently organized to undergo such abrupt intensification. Conversely, TCs have more chance to decay quickly because of their higher initial intensities. TCs are also more likely to undergo an eyewall replacement cycle and weaken significantly (Willoughby et al. 1982). Last, the mean and median of 24-h positive Dvorak-CI changes equal +1.0 (not shown), suggesting no bias with the climatological intensification rate of the Dvorak technique built on NA and WNP cases.

b. *Rapid-intensification threshold*

Figure 7 shows the cumulative frequency distribution of 24-h intensity changes ΔV_{24} for each storm category (storm intensity is evaluated at t = 0 h). To follow KD03's method, RI is defined as the 95th percentile of this ΔV_{24} distribution. The closest threshold to 95% is 94.7%, associated with an RI value of 30 kt or 15.4 m s^{-1} (Table 6). Note that the 95th percentile of ΔV_{24} is slightly smaller (around 25 kt) for depressions and higher (around 35 kt) for tropical storms (Fig. 7), indicating that systems at the tropical-storm stage have a better capacity to intensify. It seems reasonable, however, to use a unique RI threshold for all categories of systems as in KD03. On the basis of this 15.4 m s^{-1} threshold, the RI sample has an average 24-h pressure fall of 35 hPa and an average 24-h CI change of +1.9 units (Table 6), about 2 times the climatological intensification rate of the Dvorak technique.

It is interesting to note that KD03 and KD10 also found a 30-kt threshold, representing about the 94th percentile of ΔV_{24}, in their respective 1989–2000 and 1989–2006 samples. Their threshold was based on maximum 1-min sustained wind speeds. In the BT data used

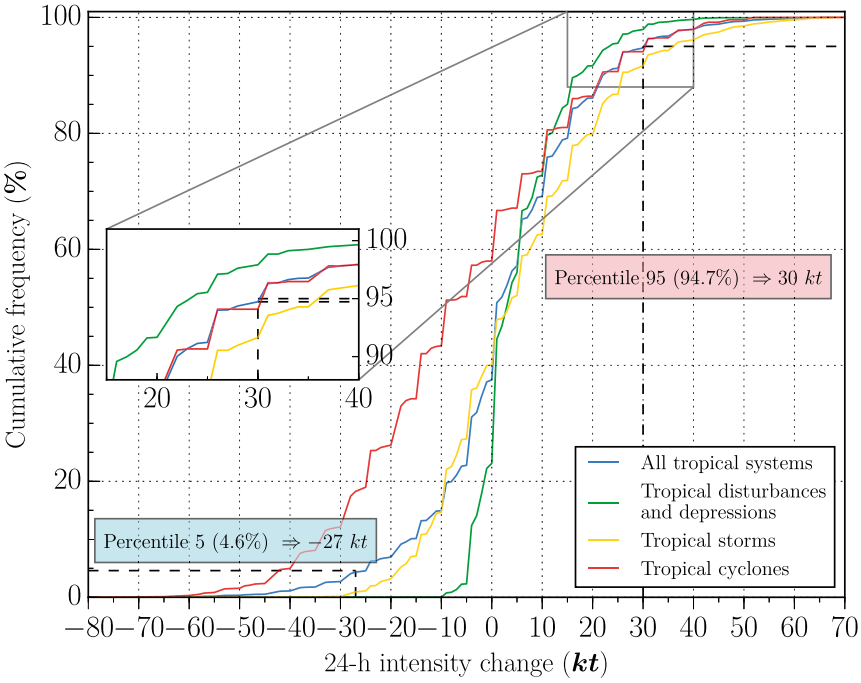

FIG. 7. Cumulative frequency distribution of overwater 24-h intensity changes (ΔV_{24}; kt) stratified by storm intensity at time $t = 0$ h during the 1999–2016 period. The total sample size is 4401.

here, each 1-min sustained estimate of peak storm intensity deduced from the Dvorak method was reduced by using a 0.88 factor to estimate the maximum 10-min mean wind speed. RI may, therefore, correspond to a higher 24-h intensity change in the SWIO basin than in the NA. This result must nevertheless be put into perspective, knowing that the HURDAT dataset benefits from aircraft reconnaissance inputs and therefore more reliable wind speed data. Table 6 gives RI thresholds derived for other percentiles of the distribution and shows that the 25-kt threshold, corresponding to the 91st percentile, is closer to the 10-min converted intensity threshold for NA systems. The 35-kt threshold corresponds to an approximate 97th percentile of ΔV_{24}, as in the NA (KD10).

Other parameters such as the central pressure or the Dvorak-CI number can be used in lieu of the maximum wind speed to diagnose storm intensity, although their relationship with storm intensity is less linear. Holliday and Thompson (1979) defined RI as a minimum 24-h pressure fall of 42 hPa over the WNP. In the current study sample, RI thresholds of −28 and −47 hPa are respectively associated with the fifth and first) percentiles of 24-h pressure changes. RIs of +2.0 and +2.5 CI correspond respectively to the 96th and 99th percentiles of 24-h CI changes. Note that a +2.5 increase of the CI number (or +2.0 if RI starts at a weak or moderate initial stage of intensity) corresponds to the maximum gain of intensity allowed by Dvorak in 24 h. A forecaster would need to break the Dvorak-CI constraints to set a higher intensification rate, which is a difficult decision to make in operations and even in postanalysis. It would have been interesting to run statistics on the Dvorak raw T number that does not have such operational constraints, but the raw T number is unfortunately not stored in RSMC La Réunion BT data.

c. *Rapid-intensification climatology*

If one defines RI with a 15.4 m s^{-1} (30 kt) threshold, the RI sample is composed of 232 cases (Table 6) from

TABLE 6. The different RI thresholds in meters per second (with knots given in parentheses) as based on overwater 24-h maximum wind speed changes (ΔV_{24}) during the 1999–2016 period. Indicated for each threshold are the RI sample size, mean 24-h pressure fall (ΔP_{24}; hPa), and mean 24-h Dvorak-CI change (ΔCI_{24}).

Percentile	Exact percentage	RI threshold	No. RI cases	Mean ΔP_{24} for RI cases	Mean ΔCI_{24} for RI cases
91	91.2	12.9 (25)	386	−29.6	1.7
95	94.7	15.4 (30)	232	−34.9	1.9
97	96.8	18.0 (35)	142	−40.3	2.1
99	98.8	23.2 (45)	51	−48.8	2.5

TABLE 7. The percentage of systems that underwent RI at least once during their lifetime as a function of the maximum intensity (VMAX; kt) attained by each system during the 1999–2016 period.

Max intensity	No. systems that underwent RI	Total no. systems	Frequency (%)
TD (VMAX < 34 kt)	0	6	0.0
Moderate TS (34 ≤ VMAX < 48 kt)	0	34	0.0
Severe TS (48 ≤ VMAX < 64 kt)	8	42	19.0
TC (64 ≤ VMAX < 90 kt)	12	27	44.4
Intense TC (90 ≤ VMAX < 116 kt)	36	41	87.8
Very intense TC (VMAX ≥ 116 kt)	14	14	100.0
All	70	164	42.7

70 systems of the total sample of 4401 cases from 164 systems. Several consecutive RI events often occur over the lifetime of the 70 tropical systems. The non-RI sample consists of 4169 cases from 94 systems. The mean 24-h intensification rate of all of the RI cases is 19.5 m s^{-1} (not shown) versus 18.2 m s^{-1} found in KD03 for the NA; that rate increases at the TS stage (20.4 m s^{-1}; not shown) in consistence with the better capacity of TSs to intensify (section 5b). An RI between t and $t + 24$ h is more frequent from an initial TS-stage intensity. An RI is observed 8.3% of the time for those systems, 2.2% of the time for initial TDs, and 5.9% of the time for initial TCs (not shown). KD03 found similar values in the NA basin, with RI occurring 4.4% of the time for TDs, 7.4% of the time for TSs, and 5.4% of the time for TCs. The fact that TDs in the SWIO experience fewer RI periods than in the NA is consistent with their average lower intensification rate (section 5a). Conversely, tropical storms are more prone to RI in the SWIO than in the NA, despite a relatively lower mean intensification rate. These figures are low as a result of the definition of RI as a rare event, occurring about 5% of the time for all tropical systems. Nevertheless, 19% of systems that attained the severe-TS stage, 44% of systems that attained TC intensity, 88% of systems that reached intense-TC strength (VMAX ≥ 46.3 m s^{-1}), and all very intense TCs (VMAX ≥ 59.6 m s^{-1}) underwent RI at least once during their lifetime (Table 7). Systems that did not exceed the moderate-TS stage (VMAX < 24.6 m s^{-1} or 48 kt) never experienced an RI period. Note that, by definition, it is impossible for a system that never exceeds the TD stage (VMAX < 34 kt) to undergo RI (+30 kt) since tropical disturbances are generally followed by RSMC La Réunion well after they reach a 4-kt intensity. Overall, 43% of all SWIO tropical systems underwent RI. Last, the proportion of midget systems that undergo RI is not significantly greater than that of nonmidget systems (Z test for two population proportions; Table 3).

The probability of RI as a function of the initial maximum wind speed of the system is mostly normal but exhibits some peaks (Fig. 8). A moving mean with a window width of 15 kt is used to smooth out some fluctuations that are possibly linked to different biases in the assignment of intensities in the various 5-kt bins (e.g., in operational practices). The smoothing highlights one peak at 65–75 kt. This peak, relating to 10-min average wind speed, is in line with what SWIO forecasters describe as the threshold above which systems can go wild. This result is also consistent with that of Xu and Wang (2015), who found that the intensification rate of NA storms is maximized for storm intensity in the 70–80-kt range (maximum 1-min sustained wind speed). They explained that such storm intensity would allow the best compromise between heating efficiency (linked to greater inner-core inertial stability) and energy dissipation caused by surface friction (linked to the cubic power of the surface wind speed). The higher propensity for systems to intensify rapidly at an initial intensity between 65 and 75 kt may therefore be associated with a real atmospheric process driving storm intensification and RI. This peak could also, in part, be induced by the application of the Dvorak technique with satellite images that do not give the same amount of detail at different storm intensities (e.g., prior vs after eyewall formation), possibly inducing biases in the assignment of storm intensities. Rapid-intensification events were not observed beyond an initial 95-kt maximum wind speed (Fig. 8), strengthening TCs up to 125 kt after 24 h. It appears that although TC Fantala (2016) in the study sample experienced RI periods at the TS and TC stages its peak 135-kt intensity did not follow an RI period. Also, as shown in Table 7, systems that never reached the severe-TS stage could not experience RI since it occurred beyond a 25-kt initial intensity, strengthening the system above 55 kt after 24 h.

The seasonal distribution of RI cases normalized by the seasonal distribution of tropical systems indicates that over the 17 cyclone seasons RI only occurred between October and May (Fig. 9). TSs have a monthly distribution with a saw-toothed shape: RI frequency decreases by one-half in November, February, and April (6%) relative to October, December, January, and March (~11%). The reason for this trend is unclear. The rapid intensification of TCs occurs preferably in March

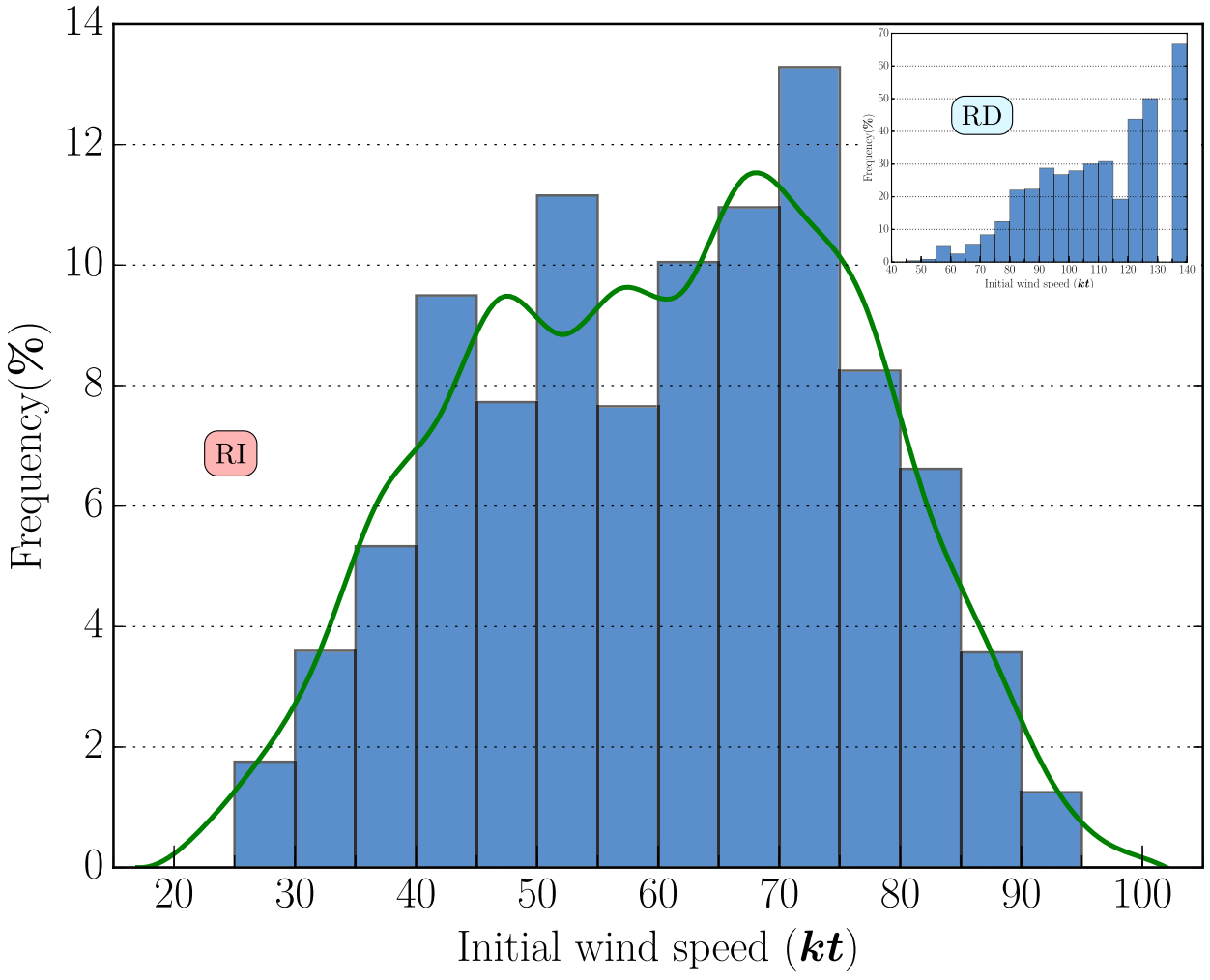

FIG. 8. The frequency of RI as a function of the maximum wind speed of systems at $t = 0$ h (VMAX; kt) during the 1999–2016 period. The frequency is obtained by dividing the number of RI cases by the total number of cases per 5-kt bin. The green line shows the smoothed frequency computed by moving average with window width of 15 kt. The inset graph shows the results obtained for RD events. The total sample size is 4401, with 232 RI cases and 201 RD cases.

and April, coinciding with the end of the warm season when SSTs are maximized. The probability of RI for TDs peaks in January before decreasing until April, suggesting that the large-scale atmospheric environment (probably atmospheric waves and humidity) may play a more important role than oceanic factors in inducing RI for tropical systems at the depression stage. Vertical wind shear is another factor that may alter the trend of RI.

Figure 10 shows the location of 24-h RI periods in the SWIO basin. Some of the 24-h tracks overlap when RI occurs for consecutive 24-h time periods. The figure indicates that RI cases are fairly evenly distributed from 50° to 95°E and are confined within the 10°–20°S latitude band with a main west-southwestward track. Very few RI cases occur southward of 20°S, which contrasts with the NA basin, where RI occurred in a 10°–38°N band over the 1989–2000 period (see Fig. 4 of KD03). This is due to frequent Rossby-wave breaking in the SWIO (Ndarana and Waugh 2010): strong, zonal, upper-level winds propagate equatorward into the subtropical latitudes and induce significant vertical wind shear in the environment of tropical systems. Despite its small extension, the Mozambique Channel favors many RI cases with RI activity shifted approximately 5° southward, following the climatologies of tropical systems (Fig. 1) and SSTs (Fig. 2). Only one system intensified rapidly below 25°S. Named Favio, this long-lived system was an exceptional phenomenon. It developed in the Chagos in mid-February of 2007 and tracked southwesterly. Boosted by an upper outflow channel linked to a powerful subtropical jet stream south of Madagascar, it

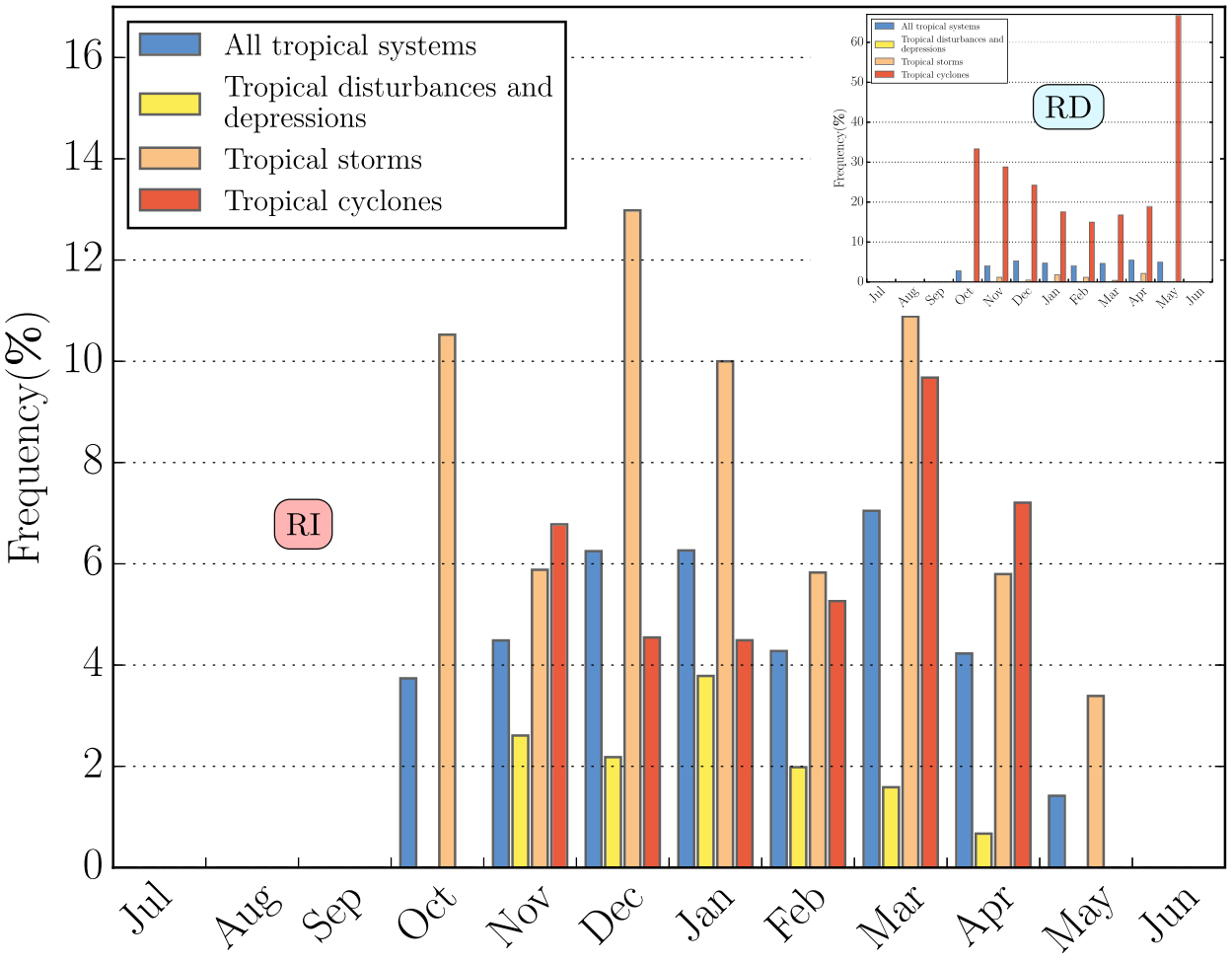

FIG. 9. Monthly distributions of RI frequency stratified by storm intensity at time $t = 0$ h during the 1999–2016 period. The abscissa spans the 12 months. The ordinate shows RI frequencies for each category of systems—(a) all, (b) TDs (VMAX $<$ 34 kt), (c) TSs (34 $\leq$ VMAX $<$ 64 kt), and (d) TCs (VMAX $\geq$ 64 kt)—obtained by dividing the number of RI cases per month in a given category by the total number of cases per month in that category. The inset graph shows the results obtained for RD events. The total sample size is 4401, with 232 RI cases and 201 RD cases.

became the most intense cyclone ever observed south of 25°S in the Mozambique Channel since the beginning of the satellite era and the first system to bear toward the northwest, that is, toward lower latitudes, after skirting the south of Madagascar.

Operational forecast errors of storm position and intensity are computed at various lead times during the 2001–16 period when forecast data were archived (Table 8). A Welch's unequal-variances one-sided t test is run to compare the mean errors between the small RI sample and the large non-RI sample at the 95% confidence level. As expected, intensity forecast errors are statistically significantly larger for RI systems, at least at short lead times until 24 h. The mean absolute error of intensity forecasts for RI systems is 10.8 m s^{-1} at 24 h since 2001 (vs 4.9 m s^{-1} for non-RI events); the mean standard deviation is also large (6.0 m s^{-1}). The average track error is significantly reduced for RI systems at 12-, 24-, and 48-h lead times. This may be because stronger systems are more easily positioned (especially prior to the use of microwave imagery and scatterometer data), allowing better model initialization and hence better track forecasts. Results indicate that the mean position error is about 120 km at 24 h over the 2001–16 period with a downward time trend (not illustrated).

d. *Rapid-decay threshold and climatology*

Similar to the RI thresholds described in section 5b for rare events, RD can be defined as the fifth percentile of the ΔV_{24} distribution. The closest threshold to 5% is 4.6% (201 of 4401 cases) and is associated with an RD value of -27 kt or -13.9 m s^{-1} (not shown). A total of

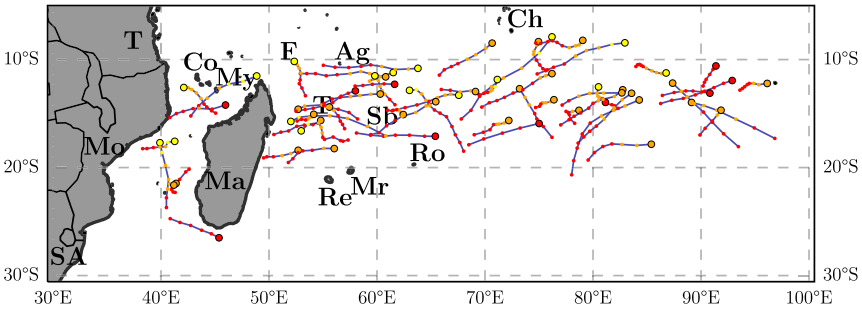

FIG. 10. The 6-h positions (colored dots) and tracks (blue segments) of RI events over the 24-h periods of RI (five consecutive dots) during the 1999–2016 period. A black circle indicates the start of a track; the systems' intensity classes are highlighted with different colors: yellow for TD (VMAX $<$ 34 kt), orange for TS (34 $\leq$ VMAX $<$ 64 kt), and red for TC (VMAX $\geq$ 64 kt). The letters are as in Fig. 1. The total sample size is 232.

276 cases (6.3% of the sample) weaken below the −25-kt threshold, and the −30-kt threshold is associated with only 179 cases (4.0% of the sample; not shown). On the basis of the $-13.9\,\mathrm{m\,s^{-1}}$ threshold, the RD sample has an average 24-h pressure increase of 34 hPa and an average 24-h CI change of −1.8 units (not shown). Note that in theory the Dvorak technique allows a maximum 2.5 decrease of the CI number. That constraint had to be broken for TC Hellen (2014), which lost 4 CI units in 24 h. An additional rule [step 9 in Dvorak (1984)] holds the CI constant for 12 h following a weakening trend. As stated in Velden et al. (2006), regional adjustments were made to ameliorate the deficiency of the Dvorak method "getting behind the intensity curve" for rapidly weakening TCs. At RSMC La Réunion, that inertia lag time may be reduced to 6 h for small systems at strong intensity, such as TC Hellen (2014).

Table 9 indicates that 10% of systems that attained the severe-TS stage, 41% of systems that attained TC intensity, 78% of systems that reached intense TC strength, and 79% of very intense TCs underwent RD at least once during their lifetime. Systems that did not exceed the moderate-TS stage never experienced an RD period (as for RI). Overall, 35% of all SWIO tropical systems underwent RD. The overall lower frequencies than those obtained for RI (Table 7) are mostly due to the different percentages used to define RD (4.6%) and RI (5.3%) events. Also, the ratio of midget systems undergoing RD is not significantly greater than that of nonmidget systems (Z test for two population proportions; Table 3).

The lower part of the cumulative frequency distribution of 24-h intensity changes (Fig. 7) indicates that the fifth percentile of ΔV_{24} is around −5 kt for depressions and around −40 kt for TCs that are characterized by a large spread of weakening rates. This result suggests that using a unique threshold for all categories of systems might not be as appropriate for RD as it is for RI.

Unlike RI, there is a mostly regular increase of RD frequency as a function of the system initial maximum wind speed (inset graph in Fig. 8); two of the three 135-kt records (associated with TC Fantala) were RD cases. There is no record of a 130-kt wind in the 17-yr dataset. The seasonal distribution of the RD cases normalized by the seasonal distribution of tropical systems clearly shows the greater propensity for TCs to rapidly decay than other categories of systems (inset graph in Fig. 9).

TABLE 8. Operational intensity forecast errors at 12-, 24-, 36-, 48-, and 60-h lead times for RI and non-RI cases from La Réunion RSMC during 15 cyclone seasons (2001/02–2015/16): absolute maximum wind error (DVmE) and root-mean-square (DVm-RMSE) error ($\mathrm{m\,s^{-1}}$), as well as direct position mean (DPE) and root-mean-square (DP-RMSE) errors for corresponding positions (km). Mean errors are highlighted in boldface when a Welch's one-sided t test reveals that they are significantly different (larger or smaller) at the 95% level, and N indicates the sample size.

	12		24		36		48		60	
Forecast time (h)	RI	Non RI	RI	Non RI	RI	Non RI	RI	Non RI	RI	Non RI
DVmE ($\mathrm{m\,s^{-1}}$)	**5.4**	**3.5**	**10.8**	**4.9**	13.5	6.4	9.0	7.6	7.7	8.2
DVm-RMSE ($\mathrm{m\,s^{-1}}$)	3.8	3.4	6.0	4.7	6.5	5.9	6.1	6.9	4.4	7.3
N	66	1973	16	1769	4	1593	4	1425	3	1247
DPE (km)	**69**	**79**	**97**	**124**	157	158	**100**	**198**	138	238
DP-RMSE (km)	49	55	52	86	60	103	64	132	92	163
N	77	2400	19	2144	4	1602	4	1439	3	1261

TABLE 9. The percentage of systems that underwent RD at least once during their lifetime as a function of the maximum intensity (VMAX; kt) attained by each system during the 1999–2016 period.

Max intensity	No. systems that underwent RD	Total no. systems	Frequency (%)
TD ($VMAX < 34$ kt)	0	6	0.0
Moderate TS (34 kt $\leq VMAX < 48$ kt)	0	34	0.0
Severe TS (48 kt $\leq VMAX < 64$ kt)	4	42	9.5
TC (64 kt $\leq VMAX < 90$ kt)	11	27	40.7
Intense TC (90 kt $\leq VMAX < 116$ kt)	32	41	78.0
Very intense TC ($VMAX \geq 116$ kt)	11	14	78.6
All	58	164	35.4

The strong role of oceanic and environmental conditions in TC RD over the SWIO is reflected by a V-shaped curve. TCs have more chance to rapidly decay at the beginning and end of the season; four of the six TC cases observed in May (67%) were rapidly decaying. This is not as evident for tropical storms.

6. Conclusions and future work

A 17-yr climatology of tropical system activity, tracks, impacts, sizes, and 24-h intensity changes is investigated in an effort to thoroughly document the southwest Indian Ocean and provide further guidance to practical storm intensity forecasts. A first formulation of the empirical maximum potential intensity of SWIO tropical systems is proposed, along with the climatology of SSTs over the basin from September to June.

A total of 165 tropical systems between the 1999/2000 and 2015/16 cyclone seasons are examined using best-track estimates from RSMC La Réunion. The coasts of Mozambique and Madagascar are the most exposed to storm hazards. Madagascar is hit two times per year by tropical systems and once every 2 years by TCs (defined by VMAX $\geq$ 64 kt or 32.9 m s^{-1}). The study then focuses on overwater tropical systems. Each year, on average, 9.7 tropical systems develop in the SWIO basin, of which 9.4 strengthen into tropical storms and 4.8 go on to become TCs that are equivalent to a hurricane or a typhoon. This represents about 11% of global tropical storm activity. More than 74% of tropical systems (81% of TCs) are observed during the wet season from December to March. Tropical systems are uniformly distributed over the basin from 35° to 95°E. TCs are mostly confined in the 10°–25°S latitude band except in the Mozambique Channel, where they occur more frequently between 15° and 30°S. The Mozambique Channel spawns systems over very warm waters (relative to the open ocean) with a position of the monsoon trough that is farther south, but these systems have very little room or time for intensification before landfall. Storm intensity in the SWIO, expressed in terms of WMO standard maximum 10-min average surface wind speed, never exceeded 69 m s^{-1} (135 kt) during the 17-yr period. Statistics on RSMC operational forecasts at 24-h lead time over the 2001–16 period indicate that the mean absolute intensity error is 5 m s^{-1} and the mean position error is about 120 km with a downward time trend.

Further guidance is provided to SWIO forecasters with the empirical MPI–SST relationship in the 22°–29°C range, derived using BT data and daily Optimum Interpolation Sea Surface Temperature analyses at 0.25° latitude–longitude resolution. It was demonstrated that the derived empirical MPI implicitly includes the effect of the outflow temperature on storm intensity. The exponential function differs from that obtained in the North Atlantic and western North Pacific Oceans (Zeng et al. 2007; Gao et al. 2016) and from the (nearly) linear relationship found in the eastern North Pacific and the Bay of Bengal. The use of EI global SST reanalyses at 0.75° spatial resolution and 6-h intervals gives a different fit with greater errors, confirming that the choice of the SST dataset can affect the MPI–SST relationship within the same basin.

The distribution of storm size, as defined by the radius of gale-force wind over the 2010–16 period or by the radius of the outermost closed isobar over the 1999–2016 period, is analyzed. Using the fifth percentile of each storm size distribution, a first statistical definition of a midget, or very small, tropical system is derived. An SWIO system can be considered to be a midget system when R34 $\leq$ 46 km. Midget systems are, on average, significantly weaker, possibly reflecting the frequent Dvorak underestimation of their intensity as noted by Lander (2004). Their mean inner-core extension is much smaller, which is consistent with their smaller R34 extension. They also experience more intensification periods than nonmidget systems. With a larger midget system sample in the future, it will be interesting to compute statistics on operational forecast errors to determine whether midget systems represent a challenge for intensity and track prediction, as is both perceived by forecasters and suggested by statistics run on the less-reliable ROCI parameter. Another possibility will be to restrict the initial intensity of all systems (e.g., 48 kt or greater) to screen out developing tropical storms that

are yet to grow, both in size and in intensity, and then see whether the midget sample maintains a lower mean intensity than the comparison group.

The distribution of 24-h overwater intensity changes is also analyzed following the method previously used for NA and ENP systems (KD03; KD10) so that comparisons can be made between basins. The distribution is less skewed toward intensification events than in the NA, probably as a result of fewer landfalls in the SWIO, increasing the likelihood of capturing most of the life cycle of systems. TCs have a mean tendency to weaken at a significantly faster rate than that found in the NA basin. This is in part because decay occurs for 60% of TC cases, versus 50% in the NA, and because the maximum decay rate for TCs over water ($-41.2\,m\,s^{-1}$ per 24 h) is significantly higher in this 17-yr period of study. The mean and median of 24-h positive Dvorak-CI changes equal +1.0, suggesting no bias with the climatological intensification rate given by the Dvorak technique that was designed on NA and WNP cases. From the 94.7th percentile of 24-h intensity changes, RI can be statistically defined in the SWIO by a minimum increase of $15.4\,m\,s^{-1}\,day^{-1}$ in the maximum surface wind speed (10-min mean). It is equal to the 30-kt official threshold determined for the NA basin using 1-min sustained winds. It also exceeds the $12.9\,m\,s^{-1}\,day^{-1}$ threshold determined for the WNP on the basis of maximum 10-min mean winds.

Rapid intensification events only occurred between October and May over the 17-yr period and were fairly evenly distributed over the SWIO basin, despite a 5° southward shift in the Mozambique Channel. Very few RI cases occurred southward of 20°S, which contrasts with the NA basin, where RI occurred in a 10°–38°N band over the 1989–2000 period (KD03). The probability of RI for TDs (VMAX < 34 kt or $17.4\,m\,s^{-1}$) peaks in January and decreases until April, suggesting that the large-scale atmospheric environment may play a more important role than oceanic factors in inducing RI for tropical systems at the depression stage. Statistics show that 43% of all tropical systems, 19% of systems that attained the severe-TS stage (VMAX ≥ 48 kt or $24.6\,m\,s^{-1}$), 44% of systems that attained TC intensity, 88% of systems that reached intense-TC strength (VMAX ≥ 90 kt or $46.3\,m\,s^{-1}$), and all very intense TCs (VMAX ≥ 116 kt or $59.6\,m\,s^{-1}$) underwent RI at least once during their lifetime. It appears that the maximum 135-kt intensity of TC Fantala (2016) in the study sample did not follow an RI period. The mean 24-h intensification rate of all RI cases in the SWIO is some 7% higher than that in the NA, and TSs (34 ≤ VMAX < 64 kt) are more prone to RI in the SWIO than in the NA. A 10-min mean maximum wind speed of 65–75 kt is the most frequent initial storm intensity for RI in the SWIO, consistent with the 70–80-kt peak in the maximum intensification rate of NA storms (maximum 1-min sustained wind speed; Xu and Wang 2015). Operational RSMC forecasts of RI events are characterized by significantly larger intensity errors at short lead times until 24 h ($10.8\,m\,s^{-1}$ at 24 h) but significantly lower track errors at 12-, 24- and 48-h lead times than non-RI events, possibly as a result of a better location of the storm center at high intensities.

Other thresholds for RI can be obtained on the basis of both central sea level pressure and changes in Dvorak CI. Thresholds of −27 and −46 hPa are thus associated with the fifth and first) percentiles, respectively, of 24-h pressure changes. Rapid intensification may also be defined by a daily increase of +2.0 and +2.5 Dvorak CI, associated respectively with the 96th and 99th percentiles of 24-h CI changes, implying that the Dvorak constraints necessarily have to be broken for systems undergoing higher intensification rates. These statistics will be useful to forecasters in the SWIO. It appears that one of the main outcomes of the ongoing reanalysis process will be that the decision making will be much less conservative with regard to the breaking of the Dvorak constraints. Six of the strongest systems of the 1999–2016 period may therefore be included in the reanalysis.

Statistics over the 17-yr period show that the average duration of the rapid-decay process is shorter than that of RI. Rapid decay for SWIO oceanic tropical systems could statistically be defined as a 24-h decrease of the maximum surface winds exceeding $13.9\,m\,s^{-1}$ (27 kt) on the basis of the 4.6th percentile of all 24-h overwater intensity changes. With that threshold, RD events would have an average 24-h pressure increase of 34 hPa and an average 24-h change in Dvorak CI of −1.8 Dvorak number. Results suggest that, unlike with RI, it is not appropriate to use a unique RD threshold for all categories of systems.

The results of this first study will be used to design a statistical–dynamical tool to predict storm intensity change or the probability of RI and to evaluate its potential use for the SWIO basin. Several sophisticated statistical techniques (neural network, decision tree, and best multilinear regression of the most relevant environmental RI predictors) will be investigated for that purpose.

As soon as the intensity reanalysis project is completed by RSMC La Réunion in the SWIO basin, future work will then focus on conducting the study over 30-yr periods (1979–2009 and 1989–2019) to address climate trends. Is there, for example, a poleward migration of the location of maximum intensity in the SWIO, similar to what was found in the global historical data over the 1982–2012 period (Kossin et al. 2014) that will affect disaster-mitigation strategies in the basin? What are the tendencies for TC maximum intensity and intensification rates over the SWIO?

Acknowledgments. We gratefully acknowledge the support of forecasters from RSMC La Réunion for the reanalysis project and their valuable input on this study. We also benefited from discussions with the climatological division of Météo-France. Funding for this research was partly provided by Grant ANR-14-CB03-0013 (SPICY). Thorough and constructive comments from two anonymous reviewers and from Dr. Roger Edson greatly improved the paper.

REFERENCES

Bister, M., and K. A. Emanuel, 1998: Dissipative heating and hurricane intensity. *Meteor. Atmos. Phys.*, **65**, 233–240, https://doi.org/10.1007/BF01030791.

Braun, S. A., 2010: Reevaluating the role of the Saharan air layer in Atlantic tropical cyclogenesis and evolution. *Mon. Wea. Rev.*, **138**, 2007–2037, https://doi.org/10.1175/2009MWR3135.1.

——, and Coauthors, 2013: NASA's Genesis and Rapid Intensification Processes (GRIP) field experiment. *Bull. Amer. Meteor. Soc.*, **94**, 345–363, https://doi.org/10.1175/BAMS-D-11-00232.1.

Brueske, K. F., and C. S. Velden, 2003: Satellite-based tropical cyclone intensity estimation using the NOAA-KLM series Advanced Microwave Sounding Unit (AMSU). *Mon. Wea. Rev.*, **131**, 687–697, https://doi.org/10.1175/1520-0493(2003)131<0687:SBTCIE>2.0.CO;2.

Carlson, T. N., and J. M. Prospero, 1972: The large-scale movement of Saharan air outbreaks over the northern equatorial Atlantic. *J. Appl. Meteor.*, **11**, 283–297, https://doi.org/10.1175/1520-0450(1972)011<0283:TLSMOS>2.0.CO;2.

Chan, J. C.-L., and R. T. Williams, 1987: Analytical and numerical studies of the beta-effect in tropical cyclone motion. Part I: Zero mean flow. *J. Atmos. Sci.*, **44**, 1257–1265, https://doi.org/10.1175/1520-0469(1987)044<1257:AANSOT>2.0.CO;2.

Chavas, D. R., and K. A. Emanuel, 2010: A QuickSCAT climatology of tropical cyclone size. *Geophys. Res. Lett.*, **37**, L18816, https://doi.org/10.1029/2010GL044558.

Courtney, J., and J. A. Knaff, 2009: Adapting the Knaff and Zehr wind–pressure relationship for operational use in tropical cyclone warning centres. *Aust. Meteor. Oceanogr. J.*, **58**, 167–179, https://doi.org/10.22499/2.5803.002.

Dee, D. P., and Coauthors, 2011: The ERA-Interim reanalysis: Configuration and performance of the data assimilation system. *Quart. J. Roy. Meteor. Soc.*, **137**, 553–597, https://doi.org/10.1002/qj.828.

DeMaria, M., and J. Kaplan, 1994a: A Statistical Hurricane Intensity Prediction Scheme (SHIPS) for the Atlantic basin. *Wea. Forecasting*, **9**, 209–220, https://doi.org/10.1175/1520-0434(1994)009<0209:ASHIPS>2.0.CO;2.

——, and ——, 1994b: Sea surface temperature and the maximum intensity of Atlantic tropical cyclones. *J. Climate*, **7**, 1324–1334, https://doi.org/10.1175/1520-0442(1994)007<1324:SSTATM>2.0.CO;2.

——, C. R. Sampson, J. A. Knaff, and K. D. Musgrave, 2014: Is tropical cyclone intensity guidance improving? *Bull. Amer. Meteor. Soc.*, **95**, 387–398, https://doi.org/10.1175/BAMS-D-12-00240.1.

Dunion, J., and C. Velden, 2004: The impact of the Saharan air layer on Atlantic tropical cyclone activity. *Bull. Amer. Meteor. Soc.*, **85**, 353–366, https://doi.org/10.1175/BAMS-85-3-353.

Duvel, J.-P., C. Basdevant, H. Bellenger, G. Reverdin, A. Vargas, and J. Vialard, 2009: The Aeroclipper: A new device to explore convective systems and cyclones. *Bull. Amer. Meteor. Soc.*, **90**, 63–72, https://doi.org/10.1175/2008BAMS2500.1.

Dvorak, V. F., 1984: Tropical cyclone intensity analysis using satellite data. NOAA Tech. Rep. NESDIS 11, 45 pp., http://severe.worldweather.wmo.int/TCFW/RAI_Training/Dvorak_1984.pdf.

Elsner, J. B., J. P. Kossin, and T. H. Jagger, 2008: The increasing intensity of the strongest tropical cyclones. *Nature*, **455**, 92–95, https://doi.org/10.1038/nature07234.

Emanuel, K. A., 1987: The dependence of hurricane intensity on climate. *Nature*, **326**, 483–485, https://doi.org/10.1038/326483a0.

——, 1988: The maximum intensity of hurricanes. *J. Atmos. Sci.*, **45**, 1143–1155, https://doi.org/10.1175/1520-0469(1988)045<1143:TMIOH>2.0.CO;2.

——, 2005: Increasing destructiveness of tropical cyclones over the past 30 years. *Nature*, **436**, 686–688, https://doi.org/10.1038/nature03906.

Fitzpatrick, P. J., 2005: *Hurricanes: A Reference Handbook*. 2nd ed. ABC-CLIO, 412 pp.

Gao, S., and L. S. Chiu, 2012: Development of Statistical Typhoon Intensity Prediction: Application to satellite-observed surface evaporation and rain rate (STIPER). *Wea. Forecasting*, **27**, 240–250, https://doi.org/10.1175/WAF-D-11-00034.1.

——, W. Zhang, J. Liu, I.-I. Lin, L. S. Chiu, and K. Cao, 2016: Improvements in typhoon intensity change classification by incorporating an ocean coupling potential intensity index into decision trees. *Wea. Forecasting*, **31**, 95–106, https://doi.org/10.1175/WAF-D-15-0062.1.

Ge, X., T. Li, and M. Peng, 2013: Effects of vertical shears and midlevel dry air on tropical cyclone developments. *J. Atmos. Sci.*, **70**, 3859–3875, https://doi.org/10.1175/JAS-D-13-066.1.

Glickman, T., Ed., 2000: *Glossary of Meteorology*. 2nd ed. Amer. Meteor. Soc., 855 pp.

Harper, B. A., S. A. Stroud, M. McCormack, and S. West, 2008: A review of historical tropical cyclone intensity in northwestern Australia and implications for climate change trend analysis. *Aust. Meteor. Mag.*, **57**, 121–141.

Harr, P. A., M. S. Kalafsky, and R. L. Elsberry, 1996: Environmental conditions prior to formation of a midget tropical cyclone during TCM-93. *Mon. Wea. Rev.*, **124**, 1693–1710, https://doi.org/10.1175/1520-0493(1996)124<1693:ECPTFO>2.0.CO;2.

Herbener, S. R., S. C. van den Heever, G. G. Carrió, S. M. Saleeby, and W. R. Cotton, 2014: Aerosol indirect effects on idealized tropical cyclone dynamics. *J. Atmos. Sci.*, **71**, 2040–2055, https://doi.org/10.1175/JAS-D-13-0202.1.

Herndon, D. C., C. S. Velden, J. Hawkins, T. Olander, and A. Wimmers, 2010: The CIMSS Satellite Consensus (SATCON) tropical cyclone intensity algorithm. *29th Conf. on Hurricanes and Tropical Meteorology*, Tucson, AZ, Amer. Meteor. Soc., 4D.4, https://ams.confex.com/ams/29Hurricanes/techprogram/paper_167959.htm.

Hoarau, K., J. Bernard, and L. Chalonge, 2012: Intense tropical cyclone activities in the northern Indian Ocean. *Int. J. Climatol.*, **32**, 1935–1945, https://doi.org/10.1002/joc.2406.

Holland, G. J., 1983: Tropical cyclone motion: Environmental interaction plus a beta effect. *J. Atmos. Sci.*, **40**, 328–342, https://doi.org/10.1175/1520-0469(1983)040<0328:TCMEIP>2.0.CO;2.

——, 1997: The maximum potential intensity of tropical cyclones. *J. Atmos. Sci.*, **54**, 2519–2541, https://doi.org/10.1175/1520-0469(1997)054<2519:TMPIOT>2.0.CO;2.

Holliday, C. R., and A. H. Thompson, 1979: Climatological characteristics of rapidly intensifying typhoons. *Mon. Wea. Rev.*, **107**, 1022–1034, https://doi.org/10.1175/1520-0493(1979)107<1022:CCORIT>2.0.CO;2.

Kaplan, J., and M. DeMaria, 2003: Large-scale characteristics of rapidly intensifying tropical cyclones in the North Atlantic basin. *Wea. Forecasting*, **18**, 1093–1108, https://doi.org/10.1175/1520-0434(2003)018<1093:LCORIT>2.0.CO;2.

——, ——, and J. A. Knaff, 2010: A revised tropical cyclone rapid intensification index for the Atlantic and eastern North Pacific basins. *Wea. Forecasting*, **25**, 220–241, https://doi.org/10.1175/2009WAF2222280.1.

Knaff, J. A., C. R. Sampson, and M. DeMaria, 2005: An operational Statistical Typhoon Intensity Prediction Scheme for the western North Pacific. *Wea. Forecasting*, **20**, 688–699, https://doi.org/10.1175/WAF863.1.

Knutson, T. R., and Coauthors, 2010: Tropical cyclones and climate change. *Nat. Geosci.*, **3**, 157–163, https://doi.org/10.1038/ngeo779.

——, and Coauthors, 2013: Dynamical downscaling projections of twenty-first-century Atlantic hurricane activity: CMIP3 and CMIP5 model-based scenarios. *J. Climate*, **26**, 6591–6617, https://doi.org/10.1175/JCLI-D-12-00539.1.

Kossin, J. P., K. A. Emanuel, and G. A. Vecchi, 2014: The poleward migration of the location of tropical cyclone maximum intensity. *Nature*, **509**, 349–352, https://doi.org/10.1038/nature13278.

Kotal, S. D., P. K. Kundu, and S. K. R. Bhowmik, 2009: An analysis of sea surface temperature and maximum potential intensity of tropical cyclones over the Bay of Bengal between 1981 and 2000. *Meteor. Appl.*, **16**, 169–177, https://doi.org/10.1002/met.96.

Lander, M. A., 2004: Monsoon depressions, monsoon gyres, midget tropical cyclones, TUTT cells, and high intensity after recurvature: Lessons learned from the use of Dvorak's techniques in the world's most prolific tropical-cyclone basin. *26th Conf. on Hurricanes and Tropical Meteorology*, Miami, FL, Amer. Meteor. Soc., 7A.5, https://ams.confex.com/ams/26HURR/techprogram/paper_75346.htm.

Lee, C.-Y., M. K. Tippett, S. J. Camargo, and A. H. Sobel, 2015: Probabilistic multiple linear regression modeling for tropical cyclone intensity. *Mon. Wea. Rev.*, **143**, 933–954, https://doi.org/10.1175/MWR-D-14-00171.1.

Merrill, R. T., 1984: A comparison of large and small tropical cyclones. *Mon. Wea. Rev.*, **112**, 1408–1418, https://doi.org/10.1175/1520-0493(1984)112<1408:ACOLAS>2.0.CO;2.

——, 1987: An experiment in statistical prediction of tropical cyclone intensity change. NOAA Tech. Memo. NWS NHC 34, 33 pp., https://www.nhc.noaa.gov/pdf/NWS-NHC-1987-34.pdf.

Ndarana, T., and D. W. Waugh, 2010: The link between cut-off lows and Rossby wave breaking in the Southern Hemisphere. *Quart. J. Roy. Meteor. Soc.*, **136**, 869–885, https://doi.org/10.1002/qj.627.

Ng, K. S. C., M. H. Lee, and Y. Zong, 2016: A re-examination of the relationship between empirical maximum potential intensity of tropical cyclone and sea surface temperature. *32nd Conf. on Hurricanes and Tropical Meteorology*, San Juan, Puerto Rico, Amer. Meteor. Soc., 10D.4, https://ams.confex.com/ams/32Hurr/webprogram/Paper293030.html.

Olander, T. L., and C. S. Velden, 2007: The advanced Dvorak technique: Continued development of an objective scheme to estimate tropical cyclone intensity using geostationary infrared satellite imagery. *Wea. Forecasting*, **22**, 287–298, https://doi.org/10.1175/WAF975.1.

Reason, C. J., and A. Keibel, 2004: Tropical Cyclone Eline and its unusual penetration and impacts over the southern African mainland. *Wea. Forecasting*, **19**, 789–805, https://doi.org/10.1175/1520-0434(2004)019<0789:TCEAIU>2.0.CO;2.

Reynolds, R. W., T. M. Smith, C. Liu, D. B. Chelton, K. S. Casey, and M. G. Schlax, 2007: Daily high-resolution-blended analyses for sea surface temperature. *J. Climate*, **20**, 5473–5496, https://doi.org/10.1175/2007JCLI1824.1.

Shu, S., F. Zhang, J. Ming, and Y. Wang, 2014: Environmental influences on the intensity changes of tropical cyclones over the western North Pacific. *Atmos. Chem. Phys.*, **14**, 6329–6342, https://doi.org/10.5194/acp-14-6329-2014.

Velden, C., and Coauthors, 2006: The Dvorak tropical cyclone intensity estimation technique: A satellite-based method that has endured for over 30 years. *Bull. Amer. Meteor. Soc.*, **87**, 1195–1210, https://doi.org/10.1175/BAMS-87-9-1195.

Vincent, E. M., M. Lengaigne, G. Madec, J. Vialard, G. Samson, N. C. Jourdain, C. E. Menkes, and S. Jullien, 2012: Processes setting the characteristics of sea surface cooling induced by tropical cyclones. *J. Geophys. Res.*, **117**, C02020, https://doi.org/10.1029/2011JC007396.

Wang, Y., Y. Rao, Z.-M. Tan, and D. Schönemann, 2015: A statistical analysis of the effects of vertical wind shear on tropical cyclone intensity change over the western North Pacific. *Mon. Wea. Rev.*, **143**, 3434–3453, https://doi.org/10.1175/MWR-D-15-0049.1.

Weatherford, C. L., and W. M. Gray, 1988a: Typhoon structure as revealed by aircraft reconnaissance. Part I: Data analysis and climatology. *Mon. Wea. Rev.*, **116**, 1032–1043, https://doi.org/10.1175/1520-0493(1988)116<1032:TSARBA>2.0.CO;2.

——, and ——, 1988b: Typhoon structure as revealed by aircraft reconnaissance. Part II: Structural variability. *Mon. Wea. Rev.*, **116**, 1044–1056, https://doi.org/10.1175/1520-0493(1988)116<1044:TSARBA>2.0.CO;2.

Whitney, L., and J. Hobgood, 1997: The relationship between sea surface temperatures and maximum intensities of tropical cyclones in the eastern North Pacific Ocean. *J. Climate*, **10**, 2921–2930, https://doi.org/10.1175/1520-0442(1997)010<2921:TRBSST>2.0.CO;2.

Willoughby, H. E., J. A. Clos, and M. G. Shoreibah, 1982: Concentric eye walls, secondary wind maxima, and the evolution of the hurricane vortex. *J. Atmos. Sci.*, **39**, 395–411, https://doi.org/10.1175/1520-0469(1982)039<0395:CEWSWM>2.0.CO;2.

WMO, 2017: Global guide to tropical cyclone forecasting. C. Guard, Ed. WMO Tech. Rep. WMO/TD-1194, 399 pp., http://www.wmo.int/cycloneguide/pdf/Global-Guide-to-Tropical-Cyclone-Forecasting.pdf.

Wood, K. M., and E. A. Ritchie, 2014: Large-scale moisture and thermodynamic properties associated with rapid weakening in the eastern North Pacific. *31st Conf. on Hurricanes and Tropical Meteorology*, San Diego, CA, Amer. Meteor. Soc., 13C.3A, https://ams.confex.com/ams/31Hurr/webprogram/Paper244326.html.

Xu, J., and Y. Wang, 2015: A statistical analysis on the dependence of tropical cyclone intensification rate on the storm intensity and size in the North Atlantic. *Wea. Forecasting*, **30**, 692–701, https://doi.org/10.1175/WAF-D-14-00141.1.

Zeng, Z.-H., Y. Wang, and C.-C. Wu, 2007: Environmental dynamical control of tropical cyclone intensity—An observational study. *Mon. Wea. Rev.*, **135**, 38–59, https://doi.org/10.1175/MWR3278.1.

——, L.-S. Chen, and Y. Wang, 2008: An observational study of environmental dynamical control of tropical cyclone intensity in the Atlantic. *Mon. Wea. Rev.*, **136**, 3307–3322, https://doi.org/10.1175/2008MWR2388.1.